Article

Discovery of [1,2,4]Triazolo[4,3-a]pyridines as Potent Inhibitors Targeting the Programmed Cell Death-1/Programmed Cell Death-Ligand 1 Interaction

Mingze Qin, Qi Cao, Shuaishuai Zheng, Ye Tian, Haotian Zhang,
Jun Xie, Hongbo Xie, Yajing Liu, Yanfang Zhao, and Ping Gong

Just Accepted

1
2
3
4
5
6
7
8
9
10
11
12
13
14
15
16
17
18
19
20
21
22
23
24
25
26
27
28
29
30
31
32
33
34
35
36
37
38
39
40
41
42
43
44
45
46
47
48
49
50
51
52
53
54
55
56
57
58
59
60

Discovery of [1,2,4]Triazolo[4,3-*a*]pyridines as Potent Inhibitors Targeting the Programmed Cell Death-1/Programmed Cell Death-Ligand 1 Interaction

Mingze Qin,*,† Qi Cao,† Shuaishuai Zheng,† Ye Tian,† Haotian Zhang,‡ Jun Xie,‡ Hongbo Xie,§ Yajing Liu,† Yanfang Zhao,*,† and Ping Gong*,†

†Key Laboratory of Structure-Based Drug Design and Discovery (Shenyang Pharmaceutical University), Ministry of Education, 103 Wenhua Road, Shenyang 110016, PR China

‡Department of Pharmacology, Shenyang Pharmaceutical University, 103 Wenhua Road, Shenyang 110016, PR China

§College of Bioinformatics Science and Technology, Harbin Medical University, Harbin 150086, PR China

ABSTRACT

Inhibition of the programmed cell death-1 (PD-1)/programmed cell death-ligand 1 (PD-L1) interaction using small-molecule inhibitors is an emerging immunotherapeutic approach. A novel series of [1,2,4]triazolo[4,3-*a*]pyridines were designed and found to be potent inhibitors of the PD-1/PD-L1 interaction. Among them, compound **A22** exhibited the most potent activity, as assessed by homogenous time-resolved fluorescence (HTRF) assay, with an IC_{50} of 92.3 nM. Furthermore, **A22** dose-dependently elevated IFN-γ production in a co-culture model of Hep3B/OS-8/hPD-L1 and CD3 T cells. We concluded that **A22** is a promising lead compound for the development of inhibitors of the PD-1/PD-L1 interaction. In

addition, we explored the structure-activity relationships of the newly synthesized [1,2,4]triazolo[4,3-*a*]pyridines, and demonstrated that a ring fusion strategy can be employed for designing analogues of the Bristol-Myers Squibb (BMS) chemical series. These studies pave the way for future drug design.

Key words: PD-1/PD-L1 interaction; rational design; structure-activity relationship; IFN-γ production.

1
2
3
4
5
6
7
8
9
10
11
12
13
14
15
16
17
18
19
20
21
22
23
24
25
26
27
28
29
30
31
32
33
34
35
36
37
38
39
40
41
42
43
44
45
46
47
48
49
50
51
52
53
54
55
56
57
58
59
60

INTRODUCTION

Immune checkpoint blockade is considered one of the most promising strategies in the field of immunotherapy.[1,2] Programmed cell death-1 (PD-1, also known as CD279) is a cell surface receptor mainly expressed on different kinds of immune system cells, particularly cytotoxic T cells.[3,4] The interaction of PD-1 with its ligands, programmed cell death-ligand 1 (PD-L1, CD274) or PD-L2 (CD273) suppresses the proliferation of T cells and the expression of inflammatory cytokines such as IL-2 and IFN-γ.[5–8] This intrinsic negative feedback system plays an important role in preventing excessive activation of T cells and in maintaining the homeostasis of immune system. PD-L1 is expressed by T cells, B cells, dendritic cells, macrophages, as well as tumor cells.[3,4] Notably, PD-L1 upregulation is found in almost 30% of solid and hematologic tumors, including melanoma, non-small cell lung cancer (NSCLC), renal cancer, and others.[6,9–13] Tumor cells utilize the PD-1/PD-L1 regulatory mechanism to avoid immunologic surveillance, which in turn facilitates their own proliferation.

Blocking the PD-1/PD-L1 interaction can restore the immune system response against tumors. To date, five humanized monoclonal antibodies (mAbs) targeting either PD-1 (nivolumab, pembrolizumab) or PD-L1 (avelumab, atezolizumab, durvalumab) have gained the U.S. Food and Drug Administration (FDA) acceptance and exhibited durable antitumor responses in a subset of patients with different cancers.[5,14] However, intrinsic disadvantages of antibody therapy such as high cost, immune-related side effects, and the lack of oral bioavailability, limit their

applications. Thus, development of small-molecule inhibitors of the PD-1/PD-L1

pathway is a promising alternative for treatment of tumor patients expressing high

levels of PD-L1.[30]

A few series of small-molecule peptides and peptidomimetics targeting the

PD-1/PD-L1 pathway have been reported.[15] CA-170 is a first-in-class, orally

bioavailable small-molecule inhibitor of PD-L1, which is currently under evaluation

in a phase-1 clinical trial in patients with advanced solid tumors and lymphomas

(NCT02812875). In addition to PD-L1, it also inhibits v-domain

immunoglobulin-containing suppressor of T cell activation (VISTA) immune

checkpoint.[16] The chemical structure of CA-170 has not been disclosed, and it is

speculated to be a peptidomimetic.

Recently, scientists from Bristol-Myers Squibb (BMS) disclosed the first class of

non-peptide small-molecule inhibitors of the PD-1/PD-L1 interaction in patent

applications, as exemplified by compounds **1**, **2**, and **6** (Figure 1).[17,18] These

compounds showed excellent inhibition of the PD-1/PD-L1 interaction in the

homogenous time-resolved fluorescence (HTRF) assay. The cocrystal structure of

human PD-L1 complexed with compound **2** was solved, revealing that PD-L1

dimerization was induced upon ligand binding.[25] Based on these results, Incyte

investigators also developed PD-1/PD-L1 pathway inhibitors characterized by an

amide fragment, such as compounds **3** and **4**.[19–21] They showed promising activity at

the biochemical level, further evaluation of these inhibitors in more experimental

models are warranted. Considering the above-described inhibitors, as well as those

designed by other groups,[15] we established a pharmacophoric model for non-peptide inhibitors of the PD-1/PD-L1 pathway, as shown in Figure 1.

Although the development of small-molecule inhibitors disrupting the PD-1/PD-L1 interaction is considered an attractive strategy worldwide, its implementation is still challenging. Pharmacodynamic as well as pharmacokinetic properties of the aforementioned non-peptide inhibitors should be investigated more comprehensively to identify a suitable candidate compound. Meanwhile, alternative inhibitors with a novel scaffold are needed for future drug design.

Here, we report the discovery of a novel series of [1,2,4]triazolo[4,3-*a*]pyridines, which potently inhibited the PD-1/PD-L1 interaction. Using a docking-based ring fusion strategy, as well as data from a preliminary study of structure-activity relationships (SARs), we devised [1,2,4]triazolo[4,3-*a*]pyridine as an attractive scaffold to develop PD-1/PD-L1 inhibitors. Detailed structural modifications were conducted accordingly, leading to the identification of compound **A22**, which exhibited a high level of inhibitory activity, as assessed by the HTRF assay, with an IC_{50} value of 92.3 nM. In addition, **A22** dose-dependently elevated IFN-γ secretion in a co-culture model of Hep3B/OS-8/hPD-L1 and CD3 T cells.
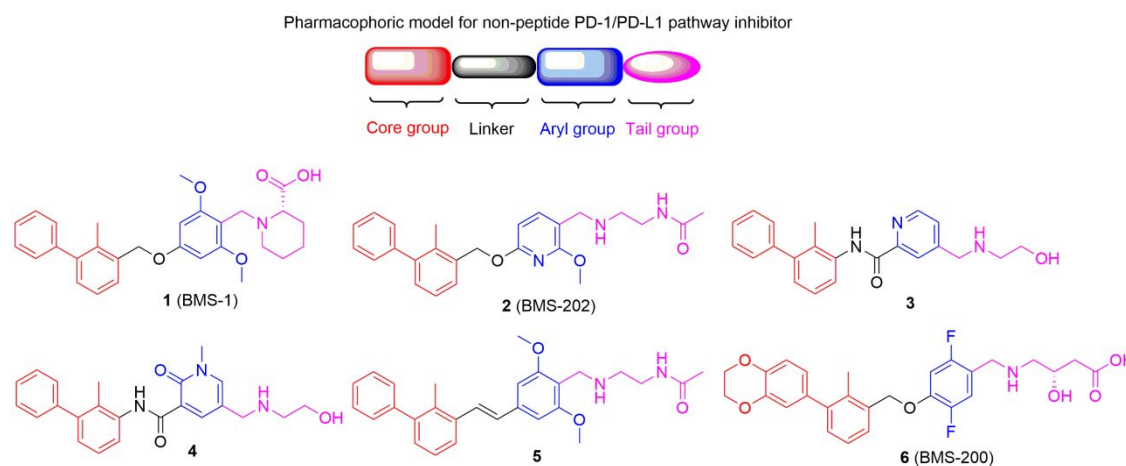
Figure 1. Pharmacophoric model and chemical structures of non-peptide PD-1/PD-L1 pathway inhibitors.

CHEMISTRY

The preparation of compounds **A4–6** and **A10–31** is described in Scheme 1. The Suzuki–Miyaura coupling between commercially available reagents **7a** and **7b** with phenylboronic acid or 2-(2,3-dihydrobenzo[b][1,4]dioxin-6-yl)-4,4,5,5-tetramethyl-1,3,2-dioxaborolane provided the intermediates **8a–c**.[19,22] The nucleophilic attack of hydrazine hydrate to methyl 5-bromo-2-chloronicotinate (**9**) gave rise to intermediate **10**, which then reacted with trimethyl orthoformate or triethyl orthoformate to yield intermediates **11a** and **11b**. A subsequent hydrolysis reaction of **11a** and **11b** yielded acids **12a** and **12b**, respectively. Intermediates **13a–d** were prepared by amidation of acids **12a** and **12b** with an appropriate amine selected from **8a–c**.[19,20] By adopting a similar coupling methodology between intermediates **13a–d** and 4,4,5,5-tetramethyl-2-vinyl-1,3,2-dioxaborolane, intermediates **14a–d** were generated, which in turn were oxidized by sodium periodate to give **15a–d**, respectively.[19,23] The

NaBH$_3$CN-mediated reductive amination was applied to convert aldehydes **15a–d** to the desired compounds, **A4–6** and **A10–31**.[17,24]

Scheme 1. Synthesis of compounds A4–6 and A10–31[a]
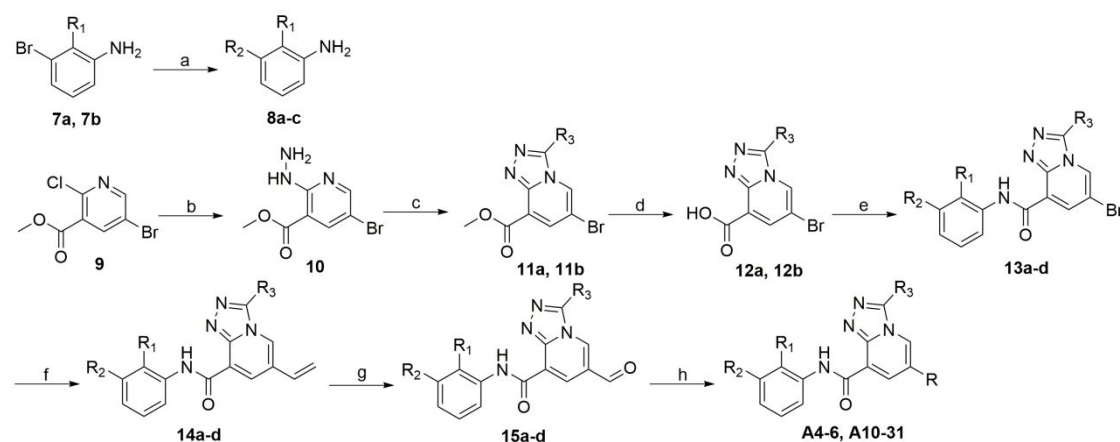
[a]Reagents and conditions: (a) phenylboronic acid, Pd(OAc)$_2$, K$_2$CO$_3$, EtOH/H$_2$O (1/1), rt, overnight, 87%, or 2-(2,3-dihydrobenzo[b][1,4]dioxin-6-yl)-4,4,5,5-tetramethyl-1,3,2-dioxaborolane, PdCl$_2$(dppf), K$_2$CO$_3$, 1,4-dioxane/H$_2$O (2/1), 100 °C, 10 h, 62%, or 2-(2,3-dihydrobenzo[b][1,4]dioxin-6-yl)-4,4,5,5-tetramethyl-1,3,2-dioxaborolane, Pd(PPh$_3$)$_4$, Cs$_2$CO$_3$, toluene/EtOH/H$_2$O (10/10/3), 95 °C, 12 h, 59%; (b) hydrazine hydrate (80%), 1,4-dioxane, 60 °C, 5 h, 80%; (c) trimethyl orthoformate or triethyl orthoformate, 100 °C, 10 h, 71–79%; (d) 1N NaOH, MeOH, reflux, 30 min, 81–87%; (e) **8a–c**, HATU, DIPEA, DMF, rt, overnight, 26–88%; (f) 4,4,5,5-tetramethyl-2-vinyl-1,3,2-dioxaborolane, PdCl$_2$(dppf), Cs$_2$CO$_3$, 1,4-dioxane/H$_2$O (20/7), 90 °C, 4 h, 47–62%; (g) OsO$_4$, NaIO$_4$, 1,4-dioxane/H$_2$O (5/1), rt, 3 h, 86–97%; (h) appropriate amine, HOAc, NaBH$_3$CN, DMF, rt, 8–24 h, 6–32%.

The synthesis of compounds **A7–9** is outlined in Scheme 2. The starting material, compound **16**, was reacted with ethane-1,2-diol to conveniently yield acetal **17**.[23] The conversion of intermediate **17** to **21** was achieved in a four-step synthetic procedure under conditions similar to those described for the preparation of intermediate **13a** from **9**. Compounds **A7–9** were obtained by deprotection of **21** in the presence of *p*-toluenesulfonic acid, followed by reductive amination using NaBH₃CN and appropriate amines.

Scheme 2. Synthesis of compounds A7–9[a]
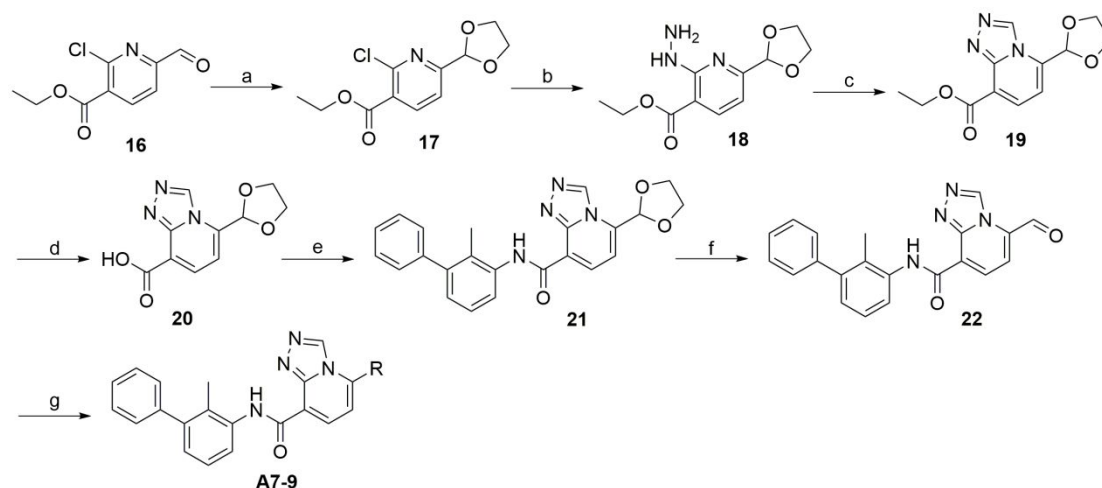
[a]Reagents and conditions: (a) ethane-1,2-diol, *p*-toluenesulfonic acid, toluene, reflux, 12 h, 67%; (b) hydrazine hydrate (80%), 1,4-dioxane, 60 °C, 7 h, 83%; (c) trimethyl orthoformate, 100 °C, 12 h, 72%; (d) 1N NaOH, methanol, reflux, 1 h, 76%; (e) **8a**, HATU, DIPEA, DMF, rt, 2 h, 89%; (f) *p*-toluenesulfonic acid, acetone/H₂O (3/2), 70 °C, 40 h, 76%; (g) appropriate amine, acetic acid, NaBH₃CN, DMF, rt, 6–12 h, 22–37%.

The synthesis of compounds **A1–3** is depicted in Scheme 3. The preparation of 6-bromoimidazo[1,2-*a*]pyridine-8-carboxylic acid (**24**) was accomplished by

cyclization of **23** with 2-chloroacetaldehyde. A sequential amidation, the Suzuki–Miyaura coupling, and oxidization reactions were utilized, which readily converted intermediate **24** to **27**. In the last step, compounds **A1–3** were prepared from **27** under NaBH$_3$CN-mediated reductive amination conditions, as described above.

Scheme 3. Synthesis of compounds A1–3^a
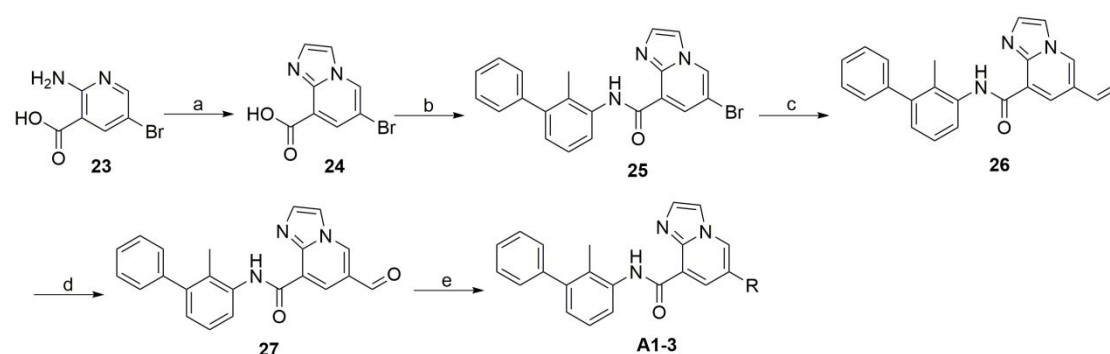
^{a}Reagents and conditions: (a) 2-chloroacetaldehyde (40%), EtOH, reflux, 7 h, 82%; (b) **8a**, HATU, DIPEA, DMF, rt, 3 h, 85%; (c) 4,4,5,5-tetramethyl-2-vinyl-1,3,2-dioxaborolane, PdCl$_2$(dppf), K$_2$CO$_3$, 1,4-dioxane/H$_2$O (4/1), 60 °C, 15 h, 53%; (d) OsO$_4$, NaIO$_4$, 1,4-dioxane/H$_2$O (5/1), rt, 2 h, 92%; (e) appropriate amine, acetic acid, NaBH$_3$CN, DMF, rt, 5–10 h, 16–21%.

RESULTS AND DISCUSSION

Structure-Based Drug Design. The crystal structure of the **2**/PD-L1 complex (PDB: 5J89) has been solved by Holak's group and represents the binding mode of inhibitors disclosed by BMS.[25,31] Based on the binding model, compound **2** is located in a deep, hydrophobic cleft formed by the dimeric PD-L1 protein. The biphenyl moiety of the inhibitor generates significant hydrophobic π-π, π-alkyl, and π-σ

interactions, with Tyr56, Met115, and Ala121. The methoxypyridine ring, which is

linked to the biphenyl moiety *via* an ether bond, substantially contributes to the

inhibitor binding mainly through strong π-π stacking with the Tyr56 residue of one

PD-L1 protein. The *N*-(2-aminoethyl)acetamide tail is oriented toward the solvent and

interacts with Asp122 and Lys124 through hydrogen bonds (Figure 2A). The

exploration of the **2**/PD-L1 complex paves the way for further development of

inhibitors of the PD-1/PD-L1 pathway. The dissection of binding mode of compound

2 to PD-L1 revealed a large space between the methoxy group and the pyridine

nitrogen, which could be occupied by an appropriate aromatic ring (Figure 2B). Thus,

a ring fusion strategy could be employed accordingly, based on the chemical structure
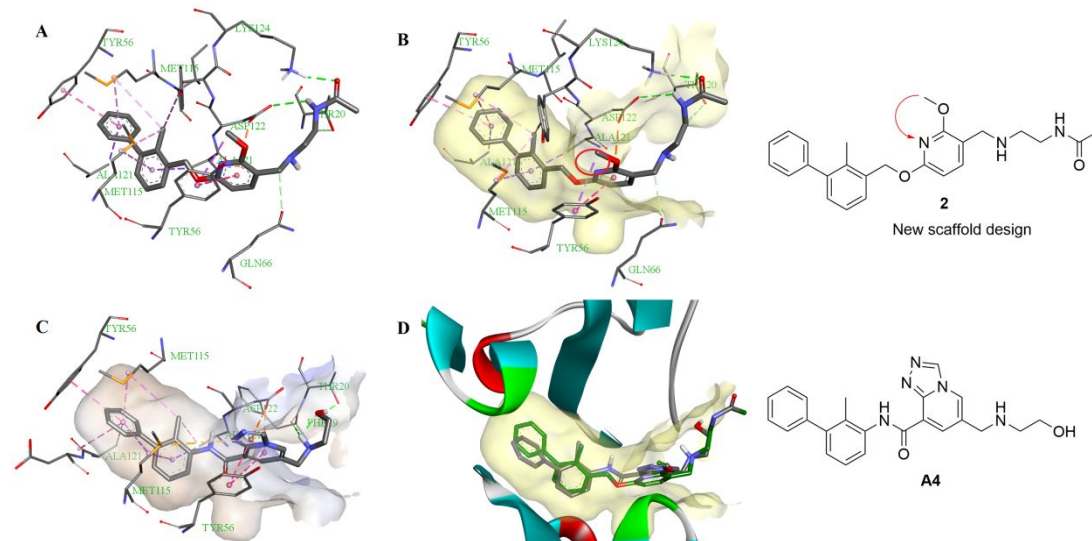
of compound **2**.

Figure 2. (A) Detailed interactions of compound **2** with the dimeric PD-L1 protein.

(B) Close-up view of compound **2** located in the hydrophobic cleft formed by the

dimeric PD-L1 protein. (C) Docking analysis of **A4** with the PD-L1 dimer. (D)

Binding overlap of **A4** and **2** in the binding site. The crystal structure of the dimeric

PD-L1 protein was taken from the RCSB Protein Data Bank (PDB: 5J89).

In addition to the ether group, the amide has been proven to be another privileged linker fragment in the design of PD-L1 inhibitors. Several series of compounds containing an amide linker were disclosed by Incyte in patent applications.[19–21] Considering the probable advantage in terms of drug-like properties, the amide was selected as the linker group in our design of new compounds.

On the basis of these considerations, we envisioned that a new [1,2,4]triazolo[4,3-*a*]pyridine or imidazo[1,2-*a*]pyridine skeleton could be established. The biphenyl moiety was retained in our initial work and was connected to a newly designed scaffold through an amide linker. Compounds **A1–9** with selected tail groups were synthesized and evaluated.
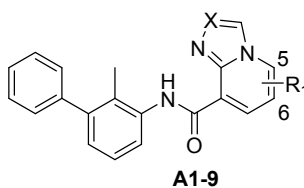
Preliminary Biochemical Evaluation of Compounds A1–9. The activities of compounds **A1–9** as inhibitors of the PD-1/PD-L1 interaction were evaluated by using the well-established HTRF assay. The biochemical data are presented as IC_{50} values and listed in Table 1.

Interestingly, [1,2,4]triazolo[4,3-*a*]pyridine compounds **A4–6** exhibited considerable activity against the PD-1/PD-L1 interaction, with IC_{50} values of 733.3, 754.7, and 1487 nM, respectively. When replacing the [1,2,4]triazolo[4,3-*a*]pyridine skeleton with an imidazo[1,2-*a*]pyridine moiety, compounds **A1–3** were clearly inactive at concentrations up to 10 μM. Considering that the hydrogen-bond interactions created by the hydrophilic tail of the inhibitor strongly contributed to inhibitor binding, we then investigated the role of tail group orientation in inhibitory
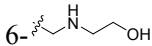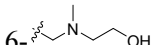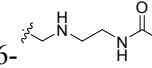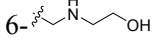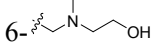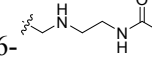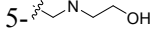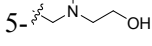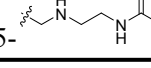
activity. Shifting the hydrophilic tails of **A4–6** from the 6- to the 5-position of [1,2,4]triazolo[4,3-*a*]pyridine gave rise to **A7–9**. However, a sharply decreased activity was observed for all three compounds, which clearly indicated that a hydrophilic group was required at the 6-position of the [1,2,4]triazolo[4,3-*a*]pyridine skeleton.

Preliminary biochemical evaluation indicated that the [1,2,4]triazolo[4,3-*a*]pyridine could serve as a privileged scaffold in the design of PD-1/PD-L1 inhibitors. To further investigate the binding mode of this chemical series and validate our design strategy, docking analysis of compound **A4** with dimeric PD-L1 was performed. As shown in Figure 2C, **A4** fitted well into the hydrophobic cleft formed by dimeric PD-L1. Regarding the biphenyl moiety, key interactions such as *π-π*, *π*-alkyl, and *π-σ* interactions with Tyr56, Met115, and Ala121, were all retained, as for compound **2**. The aminoethanol group interacted with Phe19 and Thr20 through hydrogen bonds. In addition to pyridine, the triazole moiety also formed *π-π* stacking and *π*-anion interactions with Tyr56 and Asp122, which might be beneficial for the binding of the inhibitor to dimeric PD-L1. Figure 2D shows that compounds **A4** and **2** could be well superimposed.

Table 1. Activities of compounds A1–9 in inhibition of PD-1/PD-L1 interaction.

A1-9

Compd	X	R₁	PD-1/PD-L1

			IC_{50} (nM)[a]
A1	CH	6-	>10000
A2	CH	6-	>10000
A3	CH	6-	>10000
A4	N	6-	733.3 ± 35.2
A5	N	6-	754.7 ± 27.8
A6	N	6-	1487 ± 49.3
A7	N	5-	>10000
A8	N	5-	>10000
A9	N	5-	>10000

[a]The data are generated from two independent experiments.
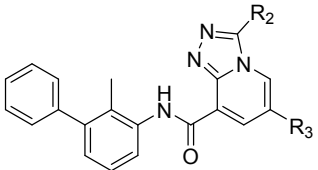
Structural Optimization of [1,2,4]Triazolo[4,3-*a*]pyridine Precursors. With the preliminary biochemical results in hand, a detailed structural optimization campaign was conducted to identify compounds with improved efficacy. At the beginning of our research, compound **1** could be easily obtained from commercial sources and thus was used as the positive control.
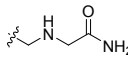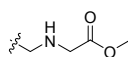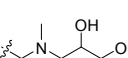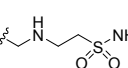
Compounds **A10–19** with diverse hydrophilic groups were prepared to further investigate the SAR of this region. In line with the preliminary docking analysis of the **A4**/PD-L1 complex, the major contribution of the tail group could derive from hydrogen-bond interactions with PD-L1. Compound **A10**, containing an amide group, showed moderate activity against the PD-1/PD-L1 interaction (IC_{50}, 2945 nM), whereas compound **A11**, with an ester group, was almost inactive. Similarly, comparisons of **A16** (IC_{50}, 5566 nM) with **A17** (IC_{50}, >10000 nM) and **A18** (IC_{50},
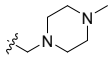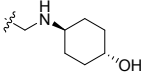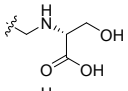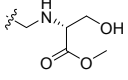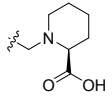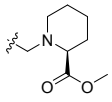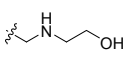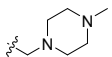
5130 nM) with **A19** (IC$_{50}$, >10000 nM) indicated that the presence of a hydrogen-bond donor resulted in higher efficacy. Compounds **A13** and **A15**, containing sulfamide and hydroxycyclohexyl fragments, exhibited promising inhibitory activity, with IC$_{50}$ values of 834 and 968.1 nM, respectively. Compound **A12**, bearing a dihydroxypropyl tail group, displayed the most potent activity, with an IC$_{50}$ value of 374.6 nM. Preliminary investigations indicated that the optimization of the tail group was straightforward, and properties such as solubility and cellular activity could be fine-tuned by modifying this region.

In order to explore the SAR of triazole, an additional methyl group was introduced to the triazole moiety of **A4** and **A14**, resulting in compounds **A20** and **A21**, respectively. However, both compounds exhibited a remarkably decreased activity, suggesting that further modification of triazole was inappropriate.

Table 2. Activities of compounds A10–21 in inhibition of PD-1/PD-L1 interaction.

Compd	R$_2$	R$_3$	PD-1/PD-L1 IC$_{50}$ (nM)[a]
A10	H		2945 ± 112.5
A11	H		>10000
A12	H		374.6 ± 13.9
A13	H		834 ± 28.6

A14	H		1347 ± 36.1
A15	H		968.1 ± 37.5
A16	H		5566 ± 138.2
A17	H		>10000
A18	H		5130 ± 95.2
A19	H		>10000
A20	Me		>10000
A21	Me		>10000
1			79.5 ± 8.6

[a]The data are generated from two independent experiments.

Also, we focused on the biphenyl moiety of newly designed [1,2,4]triazolo[4,3-*a*]pyridines. Holak et al. demonstrated that binding of the PD-L1 inhibitor **6** to PD-L1 provoked Tyr56 movement, facilitating the formation of a deep, enlarged hydrophobic tunnel, mainly induced by the 2,3-dihydro-1,4-benzodioxinyl group of compound **6**.[26] This study prompted us to synthesize compounds **A22–31** and examine whether the introduction of the 2,3-dihydro-1,4-benzodioxinyl group was beneficial to the activity of [1,2,4]triazolo[4,3-*a*]pyridine-based compounds.

Biochemical evaluation demonstrated that the incorporation of the 2,3-dihydro-1,4-benzodioxinyl moiety had a diverse impact on the activity of the different compounds. For example, both 2,3-dihydro-1,4-benzodioxinyl analogs, **A22** (IC$_{50}$, 92.3 nM) and **A23** (IC$_{50}$, 238.3 nM), containing an aminoethanol group,
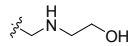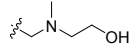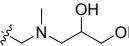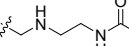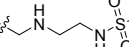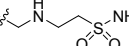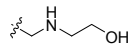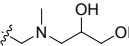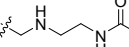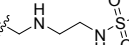
displayed significantly improved activity, as compared to the biphenyl compounds, **A4** (IC_{50}, 733.3 nM) and **A5** (IC_{50}, 754.7 nM), respectively. Similar results could be observed by comparing compound **A25** (IC_{50}, 565.8 nM) with **A6** (IC_{50}, 1487 nM). However, compound **A27** (IC_{50}, 3694 nM), bearing a sulfamide group, was less active than **A13** (IC_{50}, 834 nM). Interestingly, compound **A26** (IC_{50}, 987.8 nM), with a reverse sulfamide group, displayed a 3.74-fold higher activity compared to **A27**.

Further, modifications were conducted by replacing the methyl in the "core group" with a cyano group to investigate whether the electronic density of this region was crucial for high activity. Compounds **A24** (IC_{50}, 473.8 nM) and **A29** (IC_{50}, 486.2 nM), both bearing a dihydroxypropyl tail, exhibited comparable activity. Similar results were also observed when comparing **A26** (IC_{50}, 987.8 nM) with **A31** (IC_{50}, 983.4 nM). These findings clearly suggested that the electronic density of the "core group" was not critical for inhibitor activity. Compounds **A28** and **A30** displayed high efficacy, with IC_{50} values of 274.6 and 367 nM, respectively.

In this chemical series, compound **A22** was identified as the most promising inhibitor, demonstrating an IC_{50} of 92.3 nM, which was comparable to that of compound **1** (IC_{50}, 79.5 nM). It should be noted that **1** was unlikely to be the most active inhibitor among several hundreds of compounds reported by BMS.

Table 3. Activities of compounds A22–31 in inhibition of PD-1/PD-L1 interaction.

Journal of Medicinal Chemistry
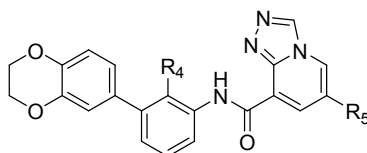
Compd	R_4	R_5	PD-1/PD-L1 IC$_{50}$ (nM)[a]
A22	Me	–NH–CH$_2$CH$_2$–OH	92.3 ± 6.2
A23	Me	–N(CH$_3$)–CH$_2$CH$_2$–OH	238.3 ± 11.7
A24	Me	–N(CH$_3$)–CH$_2$–CH(OH)–CH$_2$–OH	473.8 ± 20.1
A25	Me	–NH–CH$_2$CH$_2$–NH–C(=O)CH$_3$	565.8 ± 45.6
A26	Me	–NH–CH$_2$CH$_2$–NH–S(=O)$_2$–CH$_3$	987.8 ± 65
A27	Me	–NH–CH$_2$CH$_2$–S(=O)$_2$–NH$_2$	3694 ± 213.2
A28	CN	–NH–CH$_2$CH$_2$–OH	274.6 ± 11.7
A29	CN	–N(CH$_3$)–CH$_2$–CH(OH)–CH$_2$–OH	486.2 ± 20.3
A30	CN	–NH–CH$_2$CH$_2$–NH–C(=O)CH$_3$	367 ± 16.8
A31	CN	–NH–CH$_2$CH$_2$–NH–S(=O)$_2$–CH$_3$	983.4 ± 57.2
1			79.5 ± 8.6

[a]The data are generated from two independent experiments.

Docking analysis of A22 with dimeric PD-L1. As reported by Holak and colleagues, the 2,3-dihydro-1,4-benzodioxinyl group of compound **6** could induce a conformational change, involving a Tyr56 residue in one of the PD-L1 molecules, forming an enlarged interaction interface.[26] Thus, docking analysis of **A22** was conducted by using the **6**/PD-L1 complex (PDB: 5N2F) as a template. Figure 3A shows the interaction of **A22** with PD-L1 amino acids. The 2,3-dihydro-1,4-benzodioxinyl and central phenyl groups of **A22** established multiple key interactions with PD-L1, such as π-alkyl interactions with Met115 and π-σ interactions with Ala121, which were quite similar to those exhibited by compound **6**.

Concerning the [1,2,4]triazolo[4,3-*a*]pyridine moiety, face-to-face π-π stacking with Tyr56 and π-anion interactions with Asp122 were formed by both triazole and pyridine moieties of **A22**. The aminoethanol tail of **A22** was solvent-accessible and interacted with Ala121 *via* two hydrogen bonds.
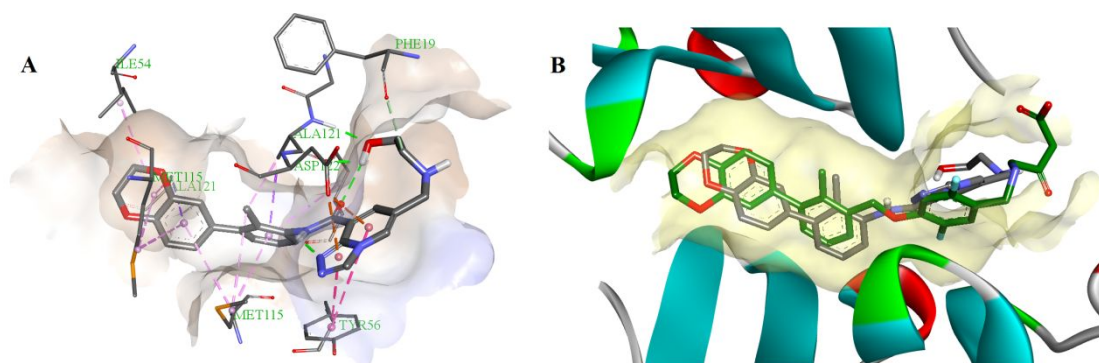
Figure 3. (A) Docking analysis of **A22** with the PD-L1 dimer. (B) Binding overlap of **A22** and **6** in the binding site. The crystal structure of the dimeric PD-L1 protein was taken from the RCSB Protein Data Bank (PDB: 5N2F).

Effect of A22 on IFN-γ production. A great number of studies have demonstrated that activation of the PD-1/PD-L1 pathway leads to numerous immunosuppressive effects, including inhibition of T cell proliferation and reduced secretion of inflammatory cytokines, such as IFN-γ.[5–8] On the other hand, blockade of the PD-1/PD-L1 interaction can enhance T cell response.[27–29] A well-established T cell-tumor co-culture assay was performed to evaluate the effects of **A22** on immune regulation. CD3 T cells isolated from peripheral blood mononuclear cells (PBMCs) were co-cultured with Hep3B cells stably expressing OS-8 (anti-CD3 single chain variable fragment) and human PD-L1, followed by the addition of **A22** and compound **1** at the indicated concentrations. IFN-γ levels were measured 72 h after stimulation.

As shown in Figure 4, **A22** significantly elevated the production of IFN-γ in a dose-dependent manner. In the presence of 5 μM **A22**, IFN-γ secretion was increased by 68.95%, which was similar to the effect induced by compound **1** (70.97%). Upon treatment with 20 μM **A22**, the IFN-γ level was increased by 205.65%.
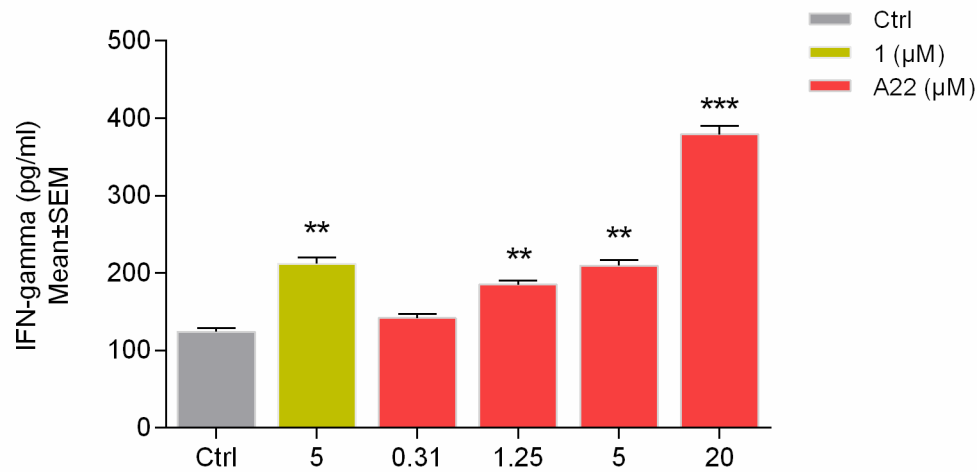
Figure 4. Effects of compounds **1** and **A22** on IFN-γ secretion from T cells co-cultured with tumor cells. Data are shown as mean ± SEM, *p<0.05, **p<0.01, *** p<0.001.

CONCLUSIONS

The development of small-molecule inhibitors has emerged as an attractive approach for the modulation of the PD-1/PD-L1 pathway, but is still in its infancy. The non-peptide inhibitors identified by scientists from BMS can serve as a promising starting point. These compounds may possess distinct pharmacokinetic and pharmacodynamic profiles from peptides, peptidomimetics, and mAbs, and deserve further investigation. Here, in an attempt to identify potent inhibitors with a novel scaffold, a docking-based ring fusion strategy was employed. A series of

[1,2,4]triazolo[4,3-*a*]pyridines were synthesized and their ability to inhibit the PD-1/PD-L1 interaction was evaluated. Among these chemicals, compound **A22** exhibited the most promising activity, with an IC_{50} value of 92.3 nM. Furthermore, **A22** significantly promoted T cell response. In a T cell-tumor co-culture assay, treatment with **A22** induced IFN-γ release in a dose-dependent manner. We explored the SARs of the newly designed [1,2,4]triazolo[4,3-*a*]pyridines and demonstrated that a fused ring could be devised for the "aryl group" moiety of the established pharmacophoric model, thus providing a valuable strategy for the rational design of PD-1/PD-L1 inhibitors.

Notably, although **A22** displayed comparable activity to the BMS compound in the cellular assay, **1** may not have been the best choice among BMS inhibitors. Compounds with higher affinities for dimeric PD-L1 would probably be more potent in cells than **A22**. In addition, compound toxicity should also be taken into account when evaluating the cellular activity. Compounds that are active in biochemical assays may be unsuitable for cell-based assays due to toxicity. More experiments should be devised to further investigate the immunoregulatory activity and toxicity of **A22**.

In conclusion, compound **A22** could be employed as a promising lead compound for the further development of blockers of the PD-1/PD-L1 interaction. We hope that non-peptide inhibitors will enter oncology clinical trials in the near future.

EXPERIMENTAL SECTION

General methods. Reagents and solvents were obtained from commercial

sources and used without further purification. All the reactions were monitored by

TLC using silica gel GF/UV 254. Flash chromatography was performed using silica

gel (300–400 mesh). Melting points were determined on a Büchi Melting Point B-540

apparatus (Büchi Labortechnik, Flawil, Switzerland). The ^{1}H and ^{13}C NMR spectra

were recorded on a Bruker AV-400 spectrometer, with TMS as an internal standard.

The low resolution of ESI-MS was recorded on an Agilent 1100 LC-MS spectrometer,

and high-resolution mass spectrometry was performed on an Agilent Accurate-Mass

Q-TOF 6530 in ESI mode. The purity of the synthesized compounds was determined

by high-performance liquid chromatography (HPLC), which was performed on an

Agilent 1260 machine with a C18 reverse-phase column (4.6 mm × 250 mm, 5 μm) at

25 °C. Mobile phase A (100% methanol) and mobile phase B (NaH_2PO_4 and H_3PO_4

buffer solution, pH = 2.5) were used in a gradient elution program (0 min, phase A:

5%, phase B: 95%; 25 min, phase A: 95%, phase B: 5%) with a flow rate of 1.0

mL/min. UV Detection was conducted at 220 nm. The purity of the target compounds

was determined to be higher than 95%.

2-Methyl-[1,1'-biphenyl]-3-amine (8a). To a mixture of

3-bromo-2-methylaniline (10 g, 54.06 mmol), phenylboronic acid (6.93 g, 56.78

mmol), K_2CO_3 (19.35 g, 140 mmol) in ethanol (70 mL) and water (70 mL) was added

$Pd(OAc)_2$ (0.73 g, 3.25 mmol). The mixture was stirred at room temperature

overnight under N_2 atmosphere. The catalyst was filtered off and the solvent was

removed by evaporation. The residue was dissolved in DCM and washed with brine.

The organic layer was dried and evaporated to afford a crude product, which was

purified by silica gel column chromatography (ethyl acetate/petroleum ether, 1/60 to

1/30) to afford compound **8a** (8.63 g, 87.2%). White solid. ^{1}H NMR (600 MHz,

DMSO-d_6) δ 7.40 (t, J = 7.6 Hz, 2H), 7.32 (t, J = 7.4 Hz, 1H), 7.25 (d, J = 7.2 Hz, 2H),

6.93 (t, J = 7.7 Hz, 1H), 6.64 (d, J = 7.9 Hz, 1H), 6.40 (d, J = 7.4 Hz, 1H), 4.92 (s,

2H), 1.92 (s, 3H). ESI-MS m/z: 184.1 [M+H]$^+$.

3-(2,3-Dihydrobenzo[*b*][1,4]dioxin-6-yl)-2-methylaniline (8b). To a mixture of

3-bromo-2-methylaniline (1.89 g, 10.21 mmol),

2-(2,3-dihydrobenzo[*b*][1,4]dioxin-6-yl)-4,4,5,5-tetramethyl-1,3,2-dioxaborolane

(4.02 g, 15.32 mmol), K_2CO_3 (4.23 g, 30.63 mmol) in 1,4-dioxane (20 mL) and water

(10 mL) was added PdCl$_2$(dppf) (0.74 g, 1.02 mmol). The mixture was stirred at 100

°C for 10 h under N_2 atmosphere. The catalyst was filtered off and the solvent was

evaporated. The residue was dissolved in DCM and washed with brine. The organic

layer was dried and evaporated to afford a crude product, which was purified by silica

gel column chromatography (ethyl acetate/petroleum ether, 1/30 to 1/10) to afford

compound **8b** (1.53 g, 62.1%). White solid. ^{1}H NMR (600 MHz, DMSO-d_6) δ 6.89

(dd, J = 15.7, 8.0 Hz, 2H), 6.70 (d, J = 12.1 Hz, 2H), 6.62 (t, J = 9.6 Hz, 1H), 6.38 (d,

J = 7.4 Hz, 1H), 4.86 (s, 2H), 4.27 (s, 4H), 1.93 (s, 3H). ESI-MS m/z: 242.1 [M+H]$^+$.

2-Amino-6-(2,3-dihydrobenzo[*b*][1,4]dioxin-6-yl)benzonitrile (8c).

2-Amino-6-bromobenzonitrile (2 g, 10.21 mmol),

2-(2,3-dihydrobenzo[*b*][1,4]dioxin-6-yl)-4,4,5,5-tetramethyl-1,3,2-dioxaborolane

(2.94 g, 11.22 mmol), Cs_2CO_3 (6.65 g, 20.4 mmol), and Pd(PPh$_3$)$_4$ (1.18 g, 1.02 mmol)

was added to a mixture of toluene (10 mL), EtOH (10 mL) and water (3 mL). The

solution was stirred at 95 °C for 12 h under N_2 atmosphere. The catalyst was filtered off and the solvent was concentrated. The residue was dissolved in DCM and washed with brine. The organic layer was dried and evaporated to afford a crude product, which was purified by silica gel column chromatography (ethyl acetate/petroleum ether, 1/20 to 1/10) to afford compound **8c** (1.51 g, 58.6%). White solid. ^{1}H NMR (600 MHz, DMSO-d_6) δ 7.30 (t, *J* = 7.9 Hz, 1H), 6.98 (s, 1H), 6.95 (d, *J* = 1.7 Hz, 2H), 6.76 (d, *J* = 8.4 Hz, 1H), 6.56 (d, *J* = 7.4 Hz, 1H), 6.05 (s, 2H), 4.29 (s, 4H). ESI-MS m/z: 253.1 [M+H]$^+$.

Methyl 5-bromo-2-hydrazinylnicotinate (10). To a mixture of intermediate **9** (12 g, 48.21 mmol) in 1,4-dioxane (60 mL) was added hydrazine hydrate (80%, 12 g, 192 mmol). The mixure was stirred at 60 °C for 5 h when TLC indicated the completion of the reaction. Being cooled to room temperature, the precipitate was filtered off to afford compound **10** (9.4 g, 79.6%). Yellow solid. ^{1}H NMR (600 MHz, DMSO-d_6) δ 8.59 (s, 1H), 8.43 (d, *J* = 1.5 Hz, 1H), 8.14 (d, *J* = 2.2 Hz, 1H), 4.52 (s, 2H), 3.83 (s, 3H). ESI-MS m/z: 246.0 [M+H]$^+$.

Methyl 6-bromo-[1,2,4]triazolo[4,3-*a*]pyridine-8-carboxylate (11a). At room temperature, intermediate **10** (5 g, 20.41 mmol) was added to trimethyl orthoformate (30 mL). The mixture was stirred at 100 °C for 10 h. Upon completion of the reaction, the solution was cooled to room temperature. The precipitate was filtered off, washed, and dried to generate compound **11a** (4.09 g, 78.6%). Off-white solid. ^{1}H NMR (600 MHz, DMSO-d_6) δ 9.29 (s, 1H), 9.19 (s, 1H), 8.03 (s, 1H), 3.95 (s, 3H). ESI-MS m/z: 256.0 [M+H]$^+$.

Compound **11b** was prepared from intermediate **10** in a similar manner as described for compound **11a**, with triethyl orthoformate replacing trimethyl orthoformate.

Methyl 6-bromo-3-methyl-[1,2,4]triazolo[4,3-*a*]pyridine-8-carboxylate (11b).

White solid. Yield, 71%. ^{1}H NMR (600 MHz, DMSO-d_6) δ 9.01 (s, 1H), 7.99 (s, 1H), 3.95 (s, 3H), 2.72 (s, 3H). ESI-MS m/z: 270.0 [M+H]$^+$.

6-Bromo-[1,2,4]triazolo[4,3-*a*]pyridine-8-carboxylic acid (12a). To a mixture of intermediate **11a** (1 g, 3.92 mmol) in methanol (10 mL) was added 1N NaOH aqueous solution (10 mL). The reaction mixture was heated to reflux for 30 min. Upon completion of the reaction, DCM (5 mL) was added, then the solution was extracted with water. The aqueous phase was acidized with 1N HCl solution to pH 5–6. The precipitate was collected *via* filtration and dried to afford compound **12a** (0.77 g, 81.2%). Yellow solid. ^{1}H NMR (600 MHz, DMSO-d_6) δ 9.27 (s, 1H), 9.15 (s, 1H), 7.97 (s, 1H). ESI-MS m/z: 242.0 [M+H]$^+$

Compound **12b** was prepared from intermediate **11b** in a similar manner as described for compound **12a**.

6-Bromo-3-methyl-[1,2,4]triazolo[4,3-*a*]pyridine-8-carboxylic acid (12b). Yellow solid. Yield, 87%. ^{1}H NMR (600 MHz, DMSO-d_6) δ 9.26 (s, 1H), 8.27 (s, 1H), 2.78 (s, 3H). ESI-MS m/z: 256.0 [M+H]$^+$

6-Bromo-*N*-(2-methyl-[1,1'-biphenyl]-3-yl)-[1,2,4]triazolo[4,3-*a*]pyridine-8-c arboxamide (13a). To a solution of **8a** (1.5 g, 8.19 mmol) and **12a** (2.07 g, 8.6 mmol) in anhydrous DMF (15 mL) was added HATU (4.67 g, 12.29 mmol), followed by

DIPEA (2.12 g, 16.38 mmol). The mixture was stirred at room temperature overnight.

Upon completion of the reaction, the mixture was poured into water. The precipitate

was collected *via* filtration, and was triturated with diethyl ether to give compound

13a (2.91 g, 87.5%). Off-yellow solid. ^{1}H NMR (600 MHz, DMSO-d_6) δ 11.37 (s,

1H), 9.41 (s, 1H), 9.22 (s, 1H), 8.19 (s,1H), 8.15 (d, J = 8.1 Hz, 1H), 7.48 (t, J = 7.5

Hz, 2H), 7.38 (td, J = 19.1, 7.6 Hz, 4H), 7.11 (d, J = 7.6 Hz, 1H), 2.34 (s, 3H).

ESI-MS m/z: 407.0 [M+H]+.

Compounds **13b–d** were prepared in a similar manner as described for

compound **13a**.

6-Bromo-3-methyl-*N*-(2-methyl-[1,1'-biphenyl]-3-yl)-[1,2,4]triazolo[4,3-*a*]py

ridine-8-carboxamide (13b). Off-yellow solid. 86% yield. ^{1}H NMR (600 MHz,

DMSO-d_6) δ 11.41 (s, 1H), 9.10 (d, J = 1.6 Hz, 1H), 8.19–8.13 (m, 2H), 7.48 (t, J =

7.5 Hz, 2H), 7.42–7.33 (m, 4H), 7.10 (d, J = 7.6 Hz, 1H), 2.76 (s, 3H), 2.33 (s, 3H).

ESI-MS m/z: 421.0 [M+H]+.

6-Bromo-*N*-(3-(2,3-dihydrobenzo[*b*][1,4]dioxin-6-yl)-2-methylphenyl)-[1,2,4]

triazolo[4,3-*a*]pyridine-8-carboxamide (13c). White solid. Yield, 79%. ^{1}H NMR

(600 MHz, DMSO-d_6) δ 11.34 (s, 1H), 9.41 (s, 1H), 9.22 (d, J = 1.7 Hz, 1H), 8.19 (d,

J = 1.7 Hz, 1H), 8.11 (d, J = 7.8 Hz, 1H), 7.31 (t, J = 7.8 Hz, 1H), 7.07 (d, J = 7.6 Hz,

1H), 6.94 (d, J = 8.2 Hz, 1H), 6.85–6.78 (m, 2H), 4.29 (s, 4H), 2.35 (s, 3H). ESI-MS

m/z: 465.0 [M+H]+.

6-Bromo-*N*-(2-cyano-3-(2,3-dihydrobenzo[*b*][1,4]dioxin-6-yl)phenyl)-[1,2,4]t

riazolo[4,3-*a*]pyridine-8-carboxamide (13d). White solid. Yield, 26%. ^{1}H NMR

(600 MHz, DMSO-d_6) δ 11.87 (s, 1H), 9.42 (s, 1H), 9.25 (s, 1H), 8.21 (d, J = 8.1 Hz, 2H), 7.80 (t, J = 8.0 Hz, 1H), 7.41 (d, J = 7.8 Hz, 1H), 7.14 (d, J = 1.7 Hz, 1H), 7.09 (dd, J = 8.2, 1.9 Hz, 1H), 7.02 (d, J = 8.3 Hz, 1H), 4.32 (s, 4H). ESI-MS m/z: 476.0 [M+H]$^+$.

N-(2-Methyl-[1,1'-biphenyl]-3-yl)-6-vinyl-[1,2,4]triazolo[4,3-a]pyridine-8-car boxamide (14a). To a mixture of **13a** (2.3 g, 5.66 mmol), 4,4,5,5-tetramethyl-2-vinyl-1,3,2-dioxaborolane (0.96 g, 6.23 mmol) in 1,4-dioxane (20 mL) and water (7 mL) was added PdCl$_2$(dppf) (0.42 g, 0.57 mmol), followed by cesium carbonate (3.32 g, 10.2 mmol). The mixture was stirred at 90 °C for 4 h under N$_2$ atmosphere. The solution was diluted with water and extracted with ethyl acetate. The organic extract was washed with brine, dried, and evaporated to give a crude product, which was purified by silica gel column chromatography (ethyl acetate/petroleum ether, 1/100 to 1/20) to afford compound **14a** (1.03 g, 51.2%). White solid. ^{1}H NMR (600 MHz, DMSO-d_6) δ 11.43 (s, 1H), 9.47 (s, 1H), 8.90 (s, 1H), 8.46 (s, 1H), 8.19 (d, J = 8.1 Hz, 1H), 7.48 (t, J = 7.5 Hz, 2H), 7.41 (d, J = 7.4 Hz, 1H), 7.39–7.33 (m, 3H), 7.10 (d, J = 7.5 Hz, 1H), 6.89 (dd, J = 17.6, 11.1 Hz, 1H), 6.06 (d, J = 17.6 Hz, 1H), 5.52 (d, J = 11.0 Hz, 1H), 2.36 (s, 3H). ESI-MS m/z: 355.2 [M+H]$^+$.

Compounds **14b–d** were prepared from **13b–d**, respectively, in a similar manner as described for compound **14a**.

3-Methyl-N-(2-methyl-[1,1'-biphenyl]-3-yl)-6-vinyl-[1,2,4]triazolo[4,3-a]pyri dine-8-carboxamide (14b). White solid. Yield, 47%. ^{1}H NMR (600 MHz, DMSO-d_6)

δ 11.46 (s, 1H), 8.74 (s, 1H), 8.42 (d, J = 1.3 Hz, 1H), 8.20 (d, J = 7.9 Hz, 1H), 7.48 (t,

J = 7.5 Hz, 2H), 7.42–7.32 (m, 4H), 7.09 (d, J = 7.5 Hz, 1H), 6.89 (dd, J = 17.6, 11.1

Hz, 1H), 6.08 (d, J = 17.6 Hz, 1H), 5.51 (d, J = 11.1 Hz, 1H), 2.76 (s, 3H), 2.34 (s,

3H). ESI-MS m/z: 369.2 [M+H]$^+$.

N-(3-(2,3-Dihydrobenzo[b][1,4]dioxin-6-yl)-2-methylphenyl)-6-vinyl-[1,2,4]triazolo[4,3-a]pyridine-8-carboxamide (14c). White solid. Yield, 62%. ^{1}H NMR (600

MHz, DMSO-d_6) δ 11.40 (s, 1H), 9.47 (s, 1H), 8.89 (s, 1H), 8.45 (s, 1H), 8.14 (d, J =

7.8 Hz, 1H), 7.31 (t, J = 7.8 Hz, 1H), 7.06 (d, J = 7.1 Hz, 1H), 6.97–6.77 (m, 4H),

6.06 (d, J = 17.6 Hz, 1H), 5.52 (d, J = 11.0 Hz, 1H), 4.29 (s, 4H), 2.36 (s, 3H).

ESI-MS m/z: 413.2 [M+H]$^+$.

N-(2-Cyano-3-(2,3-dihydrobenzo[b][1,4]dioxin-6-yl)phenyl)-6-vinyl-[1,2,4]triazolo[4,3-a]pyridine-8-carboxamide (14d). White solid. Yield, 59%. ^{1}H NMR (600

MHz, DMSO-d_6) δ 11.94 (s, 1H), 9.48 (s, 1H), 8.94 (s, 1H), 8.48 (s, 1H), 8.24 (d, J =

8.2 Hz, 1H), 7.81 (t, J = 8.0 Hz, 1H), 7.42 (d, J = 7.5 Hz, 1H), 7.15 (d, J = 2.2 Hz,

1H), 7.11 (dd, J = 8.3, 2.2 Hz, 1H), 7.03 (d, J = 8.3 Hz, 1H), 6.08 (d, J = 17.6 Hz, 1H),

5.53 (d, J = 11.0 Hz, 1H), 5.33 (t, J = 4.8 Hz, 1H), 4.33 (s, 4H). ESI-MS m/z: 424.1

[M+H]$^+$.

6-Formyl-N-(2-methyl-[1,1'-biphenyl]-3-yl)-[1,2,4]triazolo[4,3-a]pyridine-8-carboxamide (15a). Intermediate **14a** (0.65 g, 1.84 mmol) was dissolved in

1,4-dioxane (25 mL) and water (5 mL). To this mixture was added aqueous solution

of osmium tetraoxide (2% w/w in water, 3.5 mL, 0.276 mmol). After stirred for 10

min, sodium periodate (1.57 g, 7.36 mmol) was added. The mixture was stirred for

further 3 h at room temperature. The precipitate was collected *via* filtration, and dried

to give compound **15a** (0.63 g, 96.8%). Yellow solid. ^{1}H NMR (600 MHz, DMSO-d_6)

δ 11.33 (s, 1H), 10.11 (s, 1H), 9.70 (s, 1H), 9.58 (s, 1H), 8.51 (s, 1H), 8.17 (d, *J* = 7.8

Hz, 1H), 7.48 (t, *J* = 7.5 Hz, 2H), 7.41 (d, *J* = 7.4 Hz, 1H), 7.39–7.37 (m, 2H), 7.35 (d,

J = 7.9 Hz, 1H), 7.11 (d, *J* = 7.5 Hz, 1H), 2.35 (s, 3H). ESI-MS m/z: 357.1 [M+H]$^+$.

Compounds **15b–d** were prepared from **14b–d**, respectively, in a similar manner

as described for compound **15a**.

6-Formyl-3-methyl-*N*-(2-methyl-[1,1'-biphenyl]-3-yl)-[1,2,4]triazolo[4,3-*a*]py

ridine-8-carboxamide (15b). Yellow solid. Yield, 90%. ESI-MS m/z: 371.1 [M+H]$^+$.

***N*-(3-(2,3-Dihydrobenzo[*b*][1,4]dioxin-6-yl)-2-methylphenyl)-6-formyl-[1,2,4]**

triazolo[4,3-*a*]pyridine-8-carboxamide (15c). White solid. Yield, 92%. ^{1}H NMR

(600 MHz, DMSO-d_6) δ 11.30 (s, 1H), 10.11 (s, 1H), 9.69 (s, 1H), 9.58 (s, 1H), 8.50

(s, 1H), 8.13 (d, *J* = 8.0 Hz, 1H), 7.32 (t, *J* = 7.8 Hz, 1H), 7.07 (d, *J* = 7.6 Hz, 1H),

6.94 (d, *J* = 8.2 Hz, 1H), 6.88–6.77 (m, 2H), 4.29 (s, 4H), 2.36 (s, 3H). ESI-MS m/z:

415.1 [M+H]$^+$.

***N*-(2-Cyano-3-(2,3-dihydrobenzo[*b*][1,4]dioxin-6-yl)phenyl)-6-formyl-[1,2,4]t**

riazolo[4,3-*a*]pyridine-8-carboxamide (15d). White solid. Yield, 86%. ^{1}H NMR

(600 MHz, DMSO-d_6) δ 11.83 (s, 1H), 10.12 (s, 1H), 9.71 (s, 1H), 9.62 (s, 1H), 8.52

(d, *J* = 0.7 Hz, 1H), 8.24 (d, *J* = 8.3 Hz, 1H), 7.82 (t, *J* = 8.0 Hz, 1H), 7.43 (d, *J* = 7.5

Hz, 1H), 7.16 (d, *J* = 1.9 Hz, 1H), 7.11 (dd, *J* = 8.3, 2.0 Hz, 1H), 7.04 (d, *J* = 8.3 Hz,

1H), 4.33 (s, 4H). ESI-MS m/z: 426.1 [M+H]$^+$.

Ethyl 2-chloro-6-(1,3-dioxolan-2-yl)nicotinate (17). The solution of

intermediate **16** (2.5 g, 11.74 mmol), ethane-1,2-diol (1.46 g, 23.47 mmol), and

p-toluenesulfonic acid (0.48 g, 2.82 mmol) in toluene (20 mL) was stirred under

reflux for 12 h. The precipitate was collected *via* filtration, and dried to give

compound **17** (2.03 g, 67.3%). Yellow solid. ^{1}H NMR (600 MHz, DMSO-d_6) δ 8.31

(d, *J* = 7.8 Hz, 1H), 7.66 (d, *J* = 7.9 Hz, 1H), 5.78 (s, 1H), 4.36 (q, *J* = 7.1 Hz, 2H),

4.11–3.98 (m, 4H), 1.33 (t, *J* = 7.1 Hz, 3H). ESI-MS m/z: 258.1 [M+H]$^+$.

Compound **21** was prepared from intermediate **17** through a four-step synthetic

procedure which was similar to the conversion of **9** to **13a**.

5-(1,3-Dioxolan-2-yl)-*N*-(2-methyl-[1,1'-biphenyl]-3-yl)-[1,2,4]triazolo[4,3-*a*]

pyridine-8-carboxamide (21). Pale-yellow solid. Yield for four steps, 40%. ^{1}H NMR

(600 MHz, DMSO-d_6) δ 11.52 (s, 1H), 9.51 (s, 1H), 8.30 (d, *J* = 7.1 Hz, 1H), 8.19 (d,

J = 7.9 Hz, 1H), 7.48 (t, *J* = 7.5 Hz, 2H), 7.43–7.33 (m, 5H), 7.10 (d, *J* = 7.4 Hz, 1H),

6.39 (s, 1H), 4.20–4.10 (m, 4H), 2.36 (s, 3H). ESI-MS m/z: 401.2 [M+H]$^+$.

5-Formyl-*N*-(2-methyl-[1,1'-biphenyl]-3-yl)-[1,2,4]triazolo[4,3-*a*]pyridine-8-c

arboxamide (22). To a solution of intermediate **21** (1 g, 2.5 mmol) in acetone (9 mL)

and water (6 mL) was added *p*-toluenesulfonic acid (1.29 g, 7.5 mmol). The mixture

was stirred at 70 °C for 40 h. Upon completion of the reaction, the precipitate was

filtered off, and dried to give compound **22** (0.68 g, 76.3%). Yellow solid. ^{1}H NMR

(600 MHz, DMSO-d_6) δ 11.62 (s, 1H), 10.14 (s, 1H), 10.10 (s, 1H), 8.49 (d, *J* = 7.1

Hz, 1H), 8.23–8.12 (m, 2H), 7.48 (t, *J* = 7.2 Hz, 2H), 7.45–7.32 (m, 4H), 7.12 (d, *J* =

7.6 Hz, 1H), 2.37 (s, 3H). ESI-MS m/z: 357.1 [M+H]$^+$.

6-Bromoimidazo[1,2-*a*]pyridine-8-carboxylic acid (24). To a mixture of

2-amino-5-bromonicotinic acid (0.34g, 1.57 mmol) in ethanol (10 mL) was added

2-chloroacetaldehyde aqueous solution (40%, 0.68 g, 3.46 mmol). The solution was

stirred under reflux for 7 h when TLC showed the completion of the reaction. The

mixture was cooled down, the precipitate was filtered off to generate compound **24**

(0.31 g, 82.3%). Pale-yellow solid. ^{1}H NMR (600 MHz, DMSO-d_6) δ 9.46 (s, 1H),

8.31 (d, J = 5.0 Hz, 2H), 8.03 (s, 1H). ESI-MS m/z: 241.0 [M+H][+].

Compound **27** was prepared from intermediate **24** through a three-step synthetic

procedure which was similar to the conversion of **12a** to **15a**.

6-Formyl-*N*-(2-methyl-[1,1'-biphenyl]-3-yl)imidazo[1,2-*a*]pyridine-8-carbox

amide (27). White solid. Yield for three steps, 41%. ^{1}H NMR (600 MHz, DMSO-d_6)

δ 12.10 (s, 1H), 10.09 (s, 1H), 9.61 (s, 1H), 8.50 (s, 1H), 8.39 (s, 1H), 8.24 (d, J = 7.9

Hz, 1H), 7.94 (s, 1H), 7.49 (t, J = 7.4 Hz, 2H), 7.43–7.33 (m, 4H), 7.09 (d, J = 7.5 Hz,

1H), 2.36 (s, 3H). ESI-MS m/z: 356.1 [M+H][+].

6-(((2-Hydroxyethyl)amino)methyl)-*N*-(2-methyl-[1,1'-biphenyl]-3-yl)imidaz

o[1,2-*a*]pyridine-8-carboxamide (A1). To a solution of intermediate **27** (0.1 g, 0.28

mmol) and 2-aminoethan-1-ol (0.0855 g, 1.4 mmol) in DMF (8 mL) was added two

drops of acetic acid. The mixture was stirred at room temperature for 1 h, followed by

the addition of sodium cyanoborohydride (0.088 g, 1.4 mmol). Stirring was continued

for 12 h at room temperature when TLC indicated the completion of the reaction. The

solvent was evaporated to give a residue, which was purified by silica gel column

chromatography (MeOH/CH$_2$Cl$_2$, 1/200 to 1/10) to afford compound **A1** (0.019g,

16.9%). Off-white solid. Mp: 278.3–281.5 °C. ^{1}H NMR (600 MHz, DMSO-d_6) δ

12.29 (s, 1H), 8.76 (s, 1H), 8.24–8.20 (m, 2H), 8.14 (s, 1H), 7.74 (s, 1H), 7.47 (t, J =

7.4 Hz, 2H), 7.42–7.31 (m, 4H), 7.06 (d, J = 7.6 Hz, 1H), 4.53 (s, 1H), 3.84 (s, 2H),

3.50 (s, 2H), 2.62 (t, J = 5.6 Hz, 2H), 2.35 (s, 3H). ^{13}C NMR (151 MHz, DMSO-d_6) δ

161.26, 142.95, 142.41, 141.74, 137.66, 132.70, 130.21, 130.15, 129.58 (2C), 128.81,

128.64 (2C), 127.44, 126.51, 126.28, 126.25, 121.56, 120.05, 114.73, 60.62, 51.11,

49.90, 16.14. HRMS (ESI) for $C_{24}H_{24}N_4O_2$ [M + H]$^+$, calcd: 401.1972, found:

401.1975. Purity, 97.8%.

Compounds **A2–31** were prepared in a similar manner as described for

compound **A1** by reacting **15a–d**, **22** or **27** with appropriate amines.

6-(((2-Hydroxyethyl)(methyl)amino)methyl)-N-(2-methyl-[1,1'-biphenyl]-3-y

l)imidazo[1,2-a]pyridine-8-carboxamide (A2). Off-white solid. Yield, 21%. Mp:

265.5–268.3 °C. ^{1}H NMR (600 MHz, DMSO-d_6) δ 12.28 (s, 1H), 8.77 (s, 1H), 8.23 (d,

J = 8.0 Hz, 1H), 8.17 (s, 1H), 8.13 (s, 1H), 7.75 (s, 1H), 7.47 (t, J = 7.5 Hz, 2H),

7.42–7.31 (m, 4H), 7.06 (d, J = 7.4 Hz, 1H), 4.47 (t, J = 5.2 Hz, 1H), 3.63 (s, 2H),

3.57–3.53 (m, 2H), 2.53 (d, J = 6.2 Hz, 2H), 2.35 (s, 3H), 2.23 (s, 3H). ^{13}C NMR (151

MHz, DMSO-d_6) δ 161.21, 142.95, 142.46, 141.70, 137.59, 132.82, 131.62, 130.51,

130.03, 129.57 (2C), 128.66 (2C), 127.45, 126.57, 126.35, 126.27, 121.61, 120.08,

114.84, 59.21, 59.06, 58.56, 42.99, 14.32. HRMS (ESI) for $C_{25}H_{26}N_4O_2$ [M + H]$^+$,

calcd: 415.2129, found: 415.2123. Purity, 99.3%.

6-(((2-Acetamidoethyl)amino)methyl)-N-(2-methyl-[1,1'-biphenyl]-3-yl)imid

azo[1,2-a]pyridine-8-carboxamide (A3). White solid. Yield, 16%. Mp: 212.9–215.0

°C. ^{1}H NMR (600 MHz, DMSO-d_6) δ 12.28 (s, 1H), 8.77 (s, 1H), 8.23 (d, J = 7.9 Hz,

1H), 8.17 (s, 1H), 8.14 (s, 1H), 7.75 (s, 1H), 7.47 (t, J = 7.5 Hz, 2H), 7.39 (dd, J = 19.5, 7.2 Hz, 3H), 7.33 (t, J = 7.8 Hz, 1H), 7.06 (d, J = 7.5 Hz, 1H), 4.47 (s, 1H), 3.63 (s, 2H), 3.56 (d, J = 4.7 Hz, 2H), 3.37 (s, 2H), 2.35 (s, 3H), 2.23 (s, 3H). ^{13}C NMR (151 MHz, DMSO-d_6) δ 169.50, 161.26, 142.95, 142.41, 141.74, 137.67, 132.70, 130.14, 129.58 (2C), 128.69, 128.65 (2C), 127.44, 126.51, 126.28, 126.26, 125.64, 121.56, 120.07, 114.70, 49.75, 48.21, 39.06, 23.03, 16.15. HRMS (ESI) for $C_{26}H_{27}N_5O_2$ [M + H]$^+$, calcd: 442.2238, found: 442.2241. Purity, 99.2%.

6-(((2-Hydroxyethyl)amino)methyl)-*N*-(2-methyl-[1,1'-biphenyl]-3-yl)-[1,2,4] triazolo[4,3-*a*]pyridine-8-carboxamide (A4). White solid. Yield, 29%. Mp: 330.2–333.5 °C. ^{1}H NMR (400 MHz, DMSO-d_6) δ 11.41 (s, 1H), 9.20 (s, 1H), 8.77 (s, 1H), 8.56 (d, J = 1.3 Hz, 1H), 8.20 (d, J = 7.9 Hz, 1H), 7.48 (t, J = 7.3 Hz, 2H), 7.43–7.29 (m, 4H), 7.10 (d, J = 7.1 Hz, 1H), 4.63 (s, 1H), 3.99 (s, 2H), 3.52 (d, J = 4.8 Hz, 2H), 3.17 (d, J = 4.6 Hz, 1H), 2.67 (t, J = 5.7 Hz, 2H), 2.35 (s, 3H). ^{13}C NMR (151 MHz, DMSO-d_6) δ 160.13, 153.66, 147.79, 142.98, 141.60, 137.17, 134.82, 131.35, 129.57 (2C), 128.66 (2C), 127.48, 127.00, 126.67, 126.64, 126.32, 121.70, 120.23, 59.37, 58.14, 42.52, 15.93. HRMS (ESI) for $C_{23}H_{23}N_5O_2$ [M + H]$^+$, calcd: 402.1925, found: 402.1930. Purity, 99.3%.

6-(((2-Hydroxyethyl)(methyl)amino)methyl)-*N*-(2-methyl-[1,1'-biphenyl]-3-yl)-[1,2,4]triazolo[4,3-*a*]pyridine-8-carboxamide (A5). Off-white solid. Yield, 21%. Mp: 323.5–328.8 °C. ^{1}H NMR (600 MHz, DMSO-d_6) δ 11.40 (s, 1H), 9.19 (s, 1H), 8.75 (s, 1H), 8.48 (d, J = 1.3 Hz, 1H), 8.19 (d, J = 7.9 Hz, 1H), 7.48 (t, J = 7.5 Hz, 2H), 7.42–7.33 (m, 4H), 7.09 (d, J = 7.3 Hz, 1H), 4.51 (t, J = 5.4 Hz, 1H), 3.72 (s,

2H), 3.56 (q, J = 6.0 Hz, 2H), 2.54 (t, J = 6.1 Hz, 2H), 2.35 (s, 3H), 2.24 (s, 3H). [13]C

NMR (151 MHz, DMSO-d_6) δ 160.14, 153.67, 147.79, 142.99, 141.60, 137.17,

134.83, 131.36, 129.57 (2C), 128.67 (2C), 127.49, 127.00, 126.68, 126.66, 126.33,

121.72, 120.24, 59.40, 59.37, 58.14, 42.52, 15.94. HRMS (ESI) for $C_{24}H_{25}N_5O_2$ [M +

H]$^+$, calcd: 416.2081, found: 416.2077. Purity, 98.9%.

6-(((2-Acetamidoethyl)amino)methyl)-*N*-(2-methyl-[1,1'-biphenyl]-3-yl)-[1,2,
4]triazolo[4,3-*a*]pyridine-8-carboxamide (A6). Pale-yellow solid. Yield, 13%. Mp:

220.1–223.6 °C. ^{1}H NMR (600 MHz, DMSO-d_6) δ 11.40 (s, 1H), 9.16 (s, 1H), 8.75 (s,

1H), 8.53 (s, 1H), 8.19 (d, J = 8.1 Hz, 1H), 7.83 (s, 1H), 7.48 (t, J = 7.5 Hz, 2H),

7.43–7.30 (m, 4H), 7.09 (d, J = 7.5 Hz, 1H), 3.91 (s, 2H), 3.16 (dd, J = 12.1, 6.1 Hz,

2H), 2.58 (t, J = 6.4 Hz, 2H), 2.35 (s, 3H), 1.80 (s, 3H). ^{13}C NMR (151 MHz,

DMSO-d_6) δ 169.59, 160.17, 153.66, 147.65, 142.99, 141.59, 137.17, 134.54, 130.73,

130.02, 129.56 (2C), 128.67 (2C), 127.49, 126.71, 126.67, 126.34, 121.74, 120.22,

49.20, 48.06, 39.03, 23.02, 15.94. HRMS (ESI) for $C_{25}H_{26}N_6O_2$ [M + H]$^+$, calcd:

443.2190, found: 443.2193. Purity, 98.6%.

5-(((2-Hydroxyethyl)amino)methyl)-*N*-(2-methyl-[1,1'-biphenyl]-3-yl)-[1,2,4]
triazolo[4,3-*a*]pyridine-8-carboxamide (A7). Pale-yellow solid. Yield, 22%. Mp:

262.3–265.5 °C. ^{1}H NMR (600 MHz, DMSO-d_6) δ 11.54 (s, 1H), 9.64 (s, 1H), 8.28 (d,

J = 7.1 Hz, 1H), 8.20 (d, J = 8.0 Hz, 1H), 7.48 (t, J = 7.5 Hz, 2H), 7.43–7.37 (m, 3H),

7.34 (t, J = 7.9 Hz, 1H), 7.25 (d, J = 7.2 Hz, 1H), 7.09 (d, J = 7.5 Hz, 1H), 4.58 (t, J =

5.3 Hz, 1H), 4.21 (s, 2H), 3.49 (dd, J = 11.0, 5.5 Hz, 2H), 2.66 (t, J = 5.7 Hz, 2H),

2.36 (s, 3H). ^{13}C NMR (151 MHz, DMSO-d_6) δ 160.38, 147.57, 142.98, 141.69,

141.65, 137.31, 136.37, 132.46, 129.59 (2C), 128.67 (2C), 127.47, 126.71, 126.61, 126.29, 121.80, 118.16, 112.33, 60.68, 51.33, 49.30, 15.97. HRMS (ESI) for $C_{23}H_{23}N_5O_2$ [M + H]$^+$, calcd: 402.1925, found: 402.1932. Purity, 98.6%.

5-(((2-Hydroxyethyl)(methyl)amino)methyl)-*N*-(2-methyl-[1,1'-biphenyl]-3-yl)-[1,2,4]triazolo[4,3-*a*]pyridine-8-carboxamide (A8). White solid. Yield, 37%. Mp: 257.3–260.5 °C. ^{1}H NMR (600 MHz, DMSO-d_6) δ 11.55 (s, 1H), 9.72 (s, 1H), 8.26 (d, *J* = 7.1 Hz, 1H), 8.19 (d, *J* = 8.0 Hz, 1H), 7.48 (t, *J* = 7.5 Hz, 2H), 7.43–7.32 (m, 4H), 7.25 (d, *J* = 7.1 Hz, 1H), 7.09 (d, *J* = 7.5 Hz, 1H), 4.69 (t, *J* = 5.1 Hz, 1H), 4.02 (s, 2H), 3.60 (q, *J* = 5.5 Hz, 2H), 2.60 (t, *J* = 5.7 Hz, 2H), 2.36 (s, 3H), 2.22 (s, 3H). ^{13}C NMR (151 MHz, DMSO-d_6) δ 160.32, 147.60, 142.98, 141.61, 139.64, 137.24, 137.01, 132.28, 129.57 (2C), 128.68 (2C), 127.48, 126.81, 126.67, 126.30, 121.87, 118.79, 113.97, 59.56, 58.92, 57.91, 42.54, 15.97. HRMS (ESI) for $C_{24}H_{25}N_5O_2$ [M + H]$^+$, calcd: 416.2081, found: 416.2077. Purity, 97.3%.

5-(((2-Acetamidoethyl)amino)methyl)-*N*-(2-methyl-[1,1'-biphenyl]-3-yl)-[1,2,4]triazolo[4,3-*a*]pyridine-8-carboxamide (A9). White solid. Yield, 29%. Mp: 223.3–227.1 °C. ^{1}H NMR (600 MHz, DMSO-d_6) δ 11.54 (s, 1H), 9.62 (s, 1H), 8.28 (d, *J* = 7.1 Hz, 1H), 8.21 (d, *J* = 7.9 Hz, 1H), 7.82 (t, *J* = 5.0 Hz, 1H), 7.48 (t, *J* = 7.5 Hz, 2H), 7.39 (m, 3H), 7.34 (t, *J* = 7.9 Hz, 1H), 7.25 (d, *J* = 7.2 Hz, 1H), 7.09 (d, *J* = 7.4 Hz, 1H), 4.19 (s, 2H), 3.15 (s, 2H), 2.64 (t, *J* = 6.4 Hz, 2H), 2.36 (s, 3H), 1.79 (s, 3H). ^{13}C NMR (151 MHz, DMSO-d_6) δ 169.71, 160.38, 147.56, 142.99, 141.62, 141.43, 137.27, 136.35, 132.45, 129.57 (2C), 128.68 (2C), 127.48, 126.74, 126.64, 126.30, 121.83, 118.20, 112.46, 49.11, 48.43, 38.98, 22.99, 15.95. HRMS (ESI) for

$C_{25}H_{26}N_6O_2$ [M + H]$^+$, calcd: 443.2190, found: 443.2192. Purity, 98.9%.

6-(((2-Amino-2-oxoethyl)amino)methyl)-*N*-(2-methyl-[1,1'-biphenyl]-3-yl)-[1,2 ,4]triazolo[4,3-*a*]pyridine-8-carboxamide (A10). White solid. Yield, 11%. Mp: 320.1–324.3 °C. ^{1}H NMR (600 MHz, DMSO-d_6) δ 11.40 (s, 1H), 9.20 (s, 1H), 8.75 (s, 1H), 8.52 (s, 1H), 8.19 (d, *J* = 8.1 Hz, 1H), 7.48 (t, *J* = 7.5 Hz, 2H), 7.40 (t, *J* = 7.4 Hz, 1H), 7.36 (dd, *J* = 18.3, 7.9 Hz, 4H), 7.09 (d, *J* = 7.6 Hz, 1H), 7.07 (s, 1H), 3.90 (s, 2H), 3.10 (s, 2H), 2.35 (s, 3H). ^{13}C NMR (151 MHz, DMSO-d_6) δ 173.54, 160.15, 153.67, 147.68, 142.99, 141.60, 137.18, 134.52, 130.93, 129.57 (2C), 128.67 (2C), 128.13, 127.49, 126.69, 126.66, 126.33, 121.73, 120.22, 51.42, 49.41, 15.94. HRMS (ESI) for $C_{23}H_{22}N_6O_2$ [M + H]$^+$, calcd: 415.1877, found: 415.1871. Purity, 97.5%.

Methyl ((8-((2-methyl-[1,1'-biphenyl]-3-yl)carbamoyl)-[1,2,4]triazolo[4,3-*a*]pyridin-6-yl) methyl)glycinate (A11). White solid. Yield, 29%. Mp: 296.0–297.2 °C. ^{1}H NMR (600 MHz, DMSO-d_6) δ 11.39 (s, 1H), 9.13 (s, 1H), 8.74 (s, 1H), 8.53 (s, 1H), 8.19 (d, *J* = 8.1 Hz, 1H), 7.48 (t, *J* = 7.5 Hz,2H), 7.42–7.33 (m, 4H), 7.09 (d, *J* = 7.5 Hz, 1H), 3.93 (s, 2H), 3.63 (s, 3H), 3.40 (s, 2H), 2.91 (s, 1H), 2.35 (s, 3H). ^{13}C NMR (151 MHz, DMSO-d_6) δ 172.91, 160.15, 153.64, 147.70, 142.99, 141.60, 137.17, 134.61, 130.78, 129.57 (2C), 128.67 (2C), 128.07, 127.49, 126.68, 126.65, 126.33, 121.72, 120.24, 51.68, 49.51, 48.85, 15.93. HRMS (ESI) for $C_{24}H_{23}N_5O_3$ [M + H]$^+$, calcd: 430.1874, found: 430.1873. Purity, 99.0%.

6-(((2,3-Dihydroxypropyl)(methyl)amino)methyl)-*N*-(2-methyl-[1,1'-bipheny l]-3-yl)-[1,2,4]triazolo[4,3-*a*]pyridine-8-carboxamide (A12). Off-white solid. Yield,

16%. Mp: 227.5–230.8 °C. ^{1}H NMR (600 MHz, DMSO-d_6) δ 11.40 (s, 1H), 9.20 (s, 1H), 8.75 (s, 1H), 8.48 (s, 1H), 8.20 (d, J = 8.0 Hz, 1H), 7.48 (t, J = 7.5 Hz, 2H), 7.40 (t, J = 7.4 Hz, 1H), 7.37 (d, J = 7.2 Hz, 2H), 7.34 (d, J = 7.9 Hz, 1H), 7.09 (d, J = 7.5 Hz, 1H), 4.55 (s, 1H), 4.51 (s, 1H), 3.78–3.71 (m, 2H), 3.69 (dd, J = 9.8, 5.1 Hz, 1H), 3.40–3.36 (m, 1H), 3.32 (d, J = 5.8 Hz, 1H), 2.54 (dd, J = 12.8, 4.6 Hz, 1H), 2.40 (dd, J = 12.7, 7.1 Hz, 1H), 2.35 (s, 3H), 2.25 (s, 3H). ^{13}C NMR (151 MHz, DMSO-d_6) δ 160.13, 153.66, 147.79, 142.98, 141.60, 137.17, 134.85, 131.43, 129.73, 129.57 (2C), 128.66 (2C), 127.48, 126.66, 126.64, 126.32, 121.70, 120.21, 69.77, 64.92, 60.62, 58.42, 42.89, 15.94. HRMS (ESI) for $C_{25}H_{27}N_5O_3$ [M + H]$^+$, calcd: 446.2187, found: 446.2190. Purity, 98.3%.

N-(2-Methyl-[1,1'-biphenyl]-3-yl)-6-(((2-sulfamoylethyl)amino)methyl)-[1,2,4]triazolo[4,3-*a*]pyridine-8-carboxamide (A13). White solid. Yield, 23%. Mp: 278.3–281.6 °C. ^{1}H NMR (600 MHz, DMSO-d_6) δ 11.40 (s, 1H), 9.18 (s, 1H), 8.75 (s, 1H), 8.54 (t, J = 14.7 Hz, 1H), 8.21 (t, J = 15.1 Hz, 1H), 7.60–7.23 (m, 6H), 7.09 (d, J = 7.4 Hz, 1H), 6.82 (s, 2H), 3.93 (s, 2H), 3.19 (t, J = 7.1 Hz, 2H), 2.92 (t, J = 7.1 Hz, 2H), 2.35 (s, 3H), 1.23 (s, 1H). ^{13}C NMR (151 MHz, DMSO-d_6) δ 160.14, 153.68, 147.69, 142.99, 141.60, 137.17, 134.52, 130.83, 129.57 (2C), 128.67 (2C), 128.11, 127.49, 126.71, 126.67, 126.33, 121.74, 120.32, 54.69, 48.96, 43.20, 15.94. HRMS (ESI) for $C_{23}H_{24}N_6O_3S$ [M + H]$^+$, calcd: 465.1703, found: 465.1706. Purity, 99.1%.

N-(2-Methyl-[1,1'-biphenyl]-3-yl)-6-((4-methylpiperazin-1-yl)methyl)-[1,2,4]triazolo[4,3-*a*]pyridine-8-carboxamide (A14). Pale-yellow solid. Yield, 22%. Mp: 320.5–322.4 °C. ^{1}H NMR (600 MHz, DMSO-d_6) δ 11.38 (s, 1H), 9.15 (s, 1H), 8.74 (s,

1H), 8.45 (s, 1H), 8.19 (d, J = 8.0 Hz, 1H), 7.47 (t, J = 7.5 Hz, 2H), 7.43–7.28 (m, 4H), 7.08 (d, J = 7.4 Hz, 1H), 2.14 (s, 2H), 2.47 (m, 8H), 2.34 (s, 3H), 2.17 (s, 3H). ^{13}C NMR (151 MHz, DMSO-d_6) δ 160.09, 153.66, 147.80, 142.96, 141.59, 137.14, 134.75, 131.49, 129.72, 129.55 (2C), 128.65 (2C), 127.47, 126.63, 126.32, 125.98, 121.66, 120.33, 58.19, 55.01 (2C), 52.67 (2C), 46.03, 15.91. HRMS (ESI) for $C_{26}H_{28}N_6O$ [M + H]$^+$, calcd: 441.2397, found: 441.2389. Purity, 98.7%.

6-(((((1r,4r)-4-Hydroxycyclohexyl)amino)methyl)-*N*-(2-methyl-[1,1'-biphenyl] -3-yl)-[1,2,4]triazolo[4,3-*a*]pyridine-8-carboxamide (A15). White solid. Yield, 16%. Mp: 322.3–326.6 °C. ^{1}H NMR (600 MHz, DMSO-d_6) δ 11.40 (s, 1H), 9.14 (s, 1H), 8.74 (s, 1H), 8.53 (s, 1H), 8.20 (d, J = 7.8 Hz, 1H), 7.48 (t, J = 6.8 Hz, 2H), 7.43–7.32 (m, 4H), 7.10 (d, J = 7.1 Hz, 1H), 4.47 (s, 1H), 3.91 (s, 2H), 3.43 (s, 1H), 2.41 (s, 1H), 2.35 (s, 3H), 1.90 (d, J = 8.5 Hz, 2H), 1.80 (d, J = 9.3 Hz, 2H), 1.24 (s, 1H), 1.18–1.03 (m, 4H). ^{13}C NMR (151 MHz, DMSO-d_6) δ 160.19, 153.60, 147.60, 142.99, 141.61, 137.19, 134.55, 130.41, 129.57 (2C), 129.29, 128.67 (2C), 127.49, 126.67, 126.64, 126.32, 121.71, 120.13, 69.16, 55.33, 46.96, 34.19 (2C), 31.19 (2C), 15.94. HRMS (ESI) for $C_{27}H_{29}N_5O_2$ [M + H]$^+$, calcd: 456.2394, found: 456.2387. Purity, 98.6%.

((8-((2-Methyl-[1,1'-biphenyl]-3-yl)carbamoyl)-[1,2,4]triazolo[4,3-*a*]pyridin- 6-yl)methyl)-*D*-serine (A16). White solid. Yield, 9%. Mp: 248.0–252.1 °C. ^{1}H NMR (600 MHz, DMSO-d_6) δ 11.39 (s, 1H), 9.21 (s, 1H), 8.76 (s, 1H), 8.59 (s, 1H), 8.19 (d, J = 8.1 Hz, 1H), 7.48 (t, J = 7.5 Hz, 2H), 7.42–7.33 (m, 4H), 7.09 (d, J = 7.5 Hz, 1H), 4.11 (d, J = 14.0 Hz, 1H), 3.98 (d, J = 14.0 Hz, 1H), 3.66 (ddd, J = 27.3, 10.9, 5.1 Hz,

2H), 3.29 (t, J = 4.9 Hz, 1H), 2.35 (s, 3H). ^{13}C NMR (151 MHz, DMSO-d_6) δ 172.76, 160.11, 153.82, 147.80, 143.00, 141.58, 137.13, 134.95, 131.74, 129.57 (2C), 128.68 (2C), 127.50, 126.75, 126.71, 126.35, 126.10, 121.77, 120.17, 62.72, 62.20, 47.48, 15.93. HRMS (ESI) for $C_{24}H_{23}N_5O_4$ [M + H]$^+$, calcd: 446.1823, found: 446.1824. Purity, 99.1%.

Methyl ((8-((2-Methyl-[1,1'-biphenyl]-3-yl)carbamoyl)-[1,2,4]triazolo[4,3-*a*]pyridin-6-yl) methyl)-*D*-serinate (A17). White solid. Yield, 7%. Mp: 252.3–256.8 °C. ^{1}H NMR (600 MHz, DMSO-d_6) δ 11.40 (s, 1H), 9.15 (s, 1H), 8.75 (s, 1H), 8.52 (s, 1H), 8.20 (d, J = 8.1 Hz, 1H), 7.48 (t, J = 7.4 Hz, 2H), 7.42–7.33 (m, 4H), 7.09 (d, J = 7.5 Hz, 1H), 4.90 (t, J = 5.6 Hz, 1H), 4.00 (d, J = 14.0 Hz, 1H), 3.85 (d, J = 14.2 Hz, 1H), 3.65–3.59 (m, 5H), 3.37 (s, 1H), 2.83 (s, 1H), 2.35 (s, 3H). ^{13}C NMR (151 MHz, DMSO-d_6) δ 173.93, 160.16, 153.67, 147.68, 143.00, 141.59, 137.15, 134.59, 130.78, 129.56 (2C), 128.68 (2C), 128.22, 127.50, 126.72, 126.67, 126.34, 121.75, 120.18, 62.92, 62.63, 51.79, 47.76, 15.93. HRMS (ESI) for $C_{25}H_{25}N_5O_4$ [M + H]$^+$, calcd: 460.1979, found: 460.1981. Purity, 97.0%.

(*S*)-1-((8-((2-Methyl-[1,1'-biphenyl]-3-yl)carbamoyl)-[1,2,4]triazolo[4,3-*a*]py ridin-6-yl)methyl)piperidine-2-carboxylic acid (A18). White solid. Yield, 26%. Mp: 217.6–220.3 °C. ^{1}H NMR (600 MHz, DMSO-d_6) δ 11.46 (s, 1H), 9.58 (s, 1H), 8.94 (s, 1H), 8.38 (s, 1H), 8.16 (d, J = 7.7 Hz, 1H), 7.49 (d, J = 6.1 Hz, 2H), 7.43–7.34 (m, 4H), 7.11 (d, J = 7.9 Hz, 1H), 5.32 (t, J = 4.8 Hz, 1H), 3.51 (s, 2H), 3.17 (s, 2H), 2.36 (s, 3H), 1.99 (dt, J = 12.1, 6.8 Hz, 3H), 0.85 (t, J = 7.0 Hz, 3H). HRMS (ESI) for

$C_{27}H_{27}N_5O_3$ [M + H]$^+$, calcd: 470.2187, found: 470.2184. Purity, 99.5%.

Methyl

(*S*)-1-((8-((2-methyl-[1,1'-biphenyl]-3-yl)carbamoyl)-[1,2,4]triazolo[4,3-*a*]pyridin-

6-yl)methyl)piperidine-2-carboxylate (A19). White solid. Yield, 12%. Mp:

225.3.5–229.4 °C. ^{1}H NMR (600 MHz, DMSO-d_6) δ 11.47 (s, 1H), 9.44 (s, 1H), 8.71

(s, 1H), 8.27 (s, 1H), 8.18 (s, 1H), 7.48 (t, *J* = 7.2 Hz, 2H), 7.39 (dd, *J* = 17.6, 7.2 Hz,

4H), 7.09 (d, *J* = 7.4 Hz, 1H), 3.79 (d, *J* = 14.0 Hz, 1H), 3.68 (s, 3H), 3.56 (d, *J* = 13.9

Hz, 1H), 3.38 (s, 2H), 2.88 (s, 1H), 2.35 (s, 3H), 1.45 (d, *J* = 32.9 Hz, 3H), 1.23 (s,

3H). ^{13}C NMR (151 MHz, DMSO-d_6) δ 173.68, 160.26, 147.15, 143.00, 141.62,

137.78, 137.21, 134.22, 129.58 (2C), 128.68 (2C), 127.49, 126.92, 126.85, 126.72,

126.31, 125.54, 121.90, 119.34, 63.52, 56.35, 51.79, 49.13, 29.35, 25.25, 22.09, 15.96.

HRMS (ESI) for $C_{28}H_{29}N_5O_3$ [M + H]$^+$, calcd: 484.2343, found: 484.2346. Purity,

98.1%.

6-(((2-Hydroxyethyl)amino)methyl)-3-methyl-*N*-(2-methyl-[1,1'-biphenyl]-3-

yl)-[1,2,4]triazolo[4,3-*a*]pyridine-8-carboxamide (A20). White solid. Yield, 22%.

Mp: 188.7–190.2 °C. ^{1}H NMR (600 MHz, DMSO-d_6) δ 11.50 (s, 1H), 9.02 (s, 1H),

8.45 (s, 1H), 8.25 (d, *J* = 8.1 Hz, 1H), 7.48 (t, *J* = 7.5 Hz, 2H), 7.43–7.30 (m, 4H),

7.08 (d, *J* = 7.5 Hz, 1H), 4.54 (s, 1H), 3.89 (s, 2H), 3.49 (t, *J* = 5.7 Hz, 2H), 2.61 (t, *J*

= 5.7 Hz, 2H), 2.56 (s, 3H), 2.35 (s, 3H), 1.90 (s, 1H). ^{13}C NMR (151 MHz,

DMSO-d_6) δ 163.02, 160.21, 148.27, 143.00, 141.66, 137.35, 133.99, 130.18, 129.56

(2C), 128.65 (2C), 127.81, 127.46, 126.41, 126.35, 126.33, 121.22, 119.27, 60.77,

51.05, 49.48, 15.90, 14.32. HRMS (ESI) for $C_{24}H_{25}N_5O_2$ [M + H]$^+$, calcd: 416.2081,

found: 416.2086. Purity, 99.2%.

3-Methyl-*N*-(2-methyl-[1,1'-biphenyl]-3-yl)-6-((4-methylpiperazin-1-yl)meth yl)-[1,2,4]triazolo[4,3-*a*]pyridine-8-carboxamide (A21). White solid. Yield, 32%. Mp: 186.2–188.2 °C. ^{1}H NMR (600 MHz, DMSO-d_6) δ 11.50 (s, 1H), 9.03 (s, 1H), 8.39 (s, 1H), 8.24 (d, *J* = 8.1 Hz, 1H), 7.48 (t, *J* = 7.5 Hz, 2H), 7.43–7.32 (m, 4H), 7.08 (d, *J* = 7.5 Hz, 1H), 3.64 (s, 2H), 2.56 (s, 3H), 2.50–2.21 (m, 11H), 2.16 (s, 3H). ^{13}C NMR (151 MHz, DMSO-d_6) δ 163.10, 160.20, 148.46, 143.02, 141.65, 137.31, 134.28, 131.02, 129.57 (2C), 128.66 (2C), 127.47, 126.47, 126.41, 126.34, 125.22, 121.29, 119.43, 58.25, 55.04 (2C), 52.70 (2C), 46.09, 15.91, 14.34. HRMS (ESI) for $C_{27}H_{30}N_6O$ [M + H]$^+$, calcd: 455.2554, found: 455.2562. Purity, 97.3%.

N-(3-(2,3-Dihydrobenzo[*b*][1,4]dioxin-6-yl)-2-methylphenyl)-6-(((2-hydroxye thyl)amino)methyl)-[1,2,4]triazolo[4,3-*a*]pyridine-8-carboxamide (A22). Pale-yellow solid. Yield, 30%. Mp: 272.5–273.6 °C. ^{1}H NMR (600 MHz, DMSO-d_6) δ 11.37 (s, 1H), 9.16 (s, 1H), 8.74 (s, 1H), 8.52 (s, 1H), 8.15 (d, *J* = 7.9 Hz, 1H), 7.30 (t, *J* = 7.5 Hz, 1H), 7.05 (d, *J* = 7.4 Hz, 1H), 6.93 (d, *J* = 8.1 Hz, 1H), 6.85–6.78 (m, 2H), 4.52 (s, 1H), 4.29 (s, 4H), 3.92 (s, 2H), 3.49 (d, *J* = 4.9 Hz, 2H), 2.61 (t, *J* = 4.9 Hz, 2H), 2.35 (s, 3H), 1.23 (s, 1H). ^{13}C NMR (151 MHz, DMSO-d_6) δ 160.15, 153.65, 147.66, 143.40, 142.99, 142.46, 137.11, 134.72, 134.55, 130.72, 128.53, 126.85, 126.68, 126.22, 122.54, 121.57, 120.21, 118.14, 117.18, 64.49 (2C), 60.75, 51.04, 49.43, 15.96. HRMS (ESI) for $C_{25}H_{25}N_5O_4$ [M + H]$^+$, calcd: 460.1979, found: 460.1983. Purity, 98.5%.

N-(3-(2,3-Dihydrobenzo[*b*][1,4]dioxin-6-yl)-2-methylphenyl)-6-(((2-hydroxye

thyl)(methyl)amino)methyl)-[1,2,4]triazolo[4,3-*a*]pyridine-8-carboxamide (A23).

Off-white solid. Yield, 16%. Mp: 257.4–260.2 °C. ^{1}H NMR (600 MHz, DMSO-d_6) δ

11.37 (s, 1H), 9.20 (s, 1H), 8.75 (s, 1H), 8.47 (s, 1H), 8.14 (d, J = 7.8 Hz, 1H), 7.30 (t,

J = 7.7 Hz, 1H), 7.05 (d, J = 7.4 Hz, 1H), 6.93 (d, J = 8.1 Hz, 1H), 6.85–6.79 (m, 2H),

4.50 (s, 1H), 4.29 (s, 4H), 3.72 (s, 2H), 3.56 (d, J = 5.5 Hz, 2H), 2.35 (s, 3H), 2.23 (s,

3H), 1.23 (s, 2H). ^{13}C NMR (151 MHz, DMSO-d_6) δ 160.13, 153.68, 147.80, 143.40,

142.99, 142.47, 137.10, 134.83, 134.72, 131.36, 127.00, 126.86, 126.69, 126.23,

122.54, 121.58, 120.25, 118.14, 117.18, 64.48 (2C), 59.40, 59.37, 58.13, 42.52, 15.96.

HRMS (ESI) for $C_{26}H_{27}N_5O_4$ [M + H]$^+$, calcd: 474.2136, found: 474.2139. Purity,

99.5%.

_N_-(3-(2,3-Dihydrobenzo[*b*][1,4]dioxin-6-yl)-2-methylphenyl)-6-(((2,3-dihydr

oxypropyl)(methyl)amino)methyl)-[1,2,4]triazolo[4,3-*a*]pyridine-8-carboxamide

(A24). White solid. Yield, 11%. Mp: 304.5–307.8 °C. ^{1}H NMR (600 MHz, DMSO-d_6)

δ 11.38 (s, 1H), 9.20 (s, 1H), 8.75 (s, 1H), 8.48 (s, 1H), 8.15 (d, J = 8.0 Hz, 1H), 7.30

(t, J = 7.8 Hz, 1H), 7.05 (d, J = 7.5 Hz, 1H), 6.93 (d, J = 8.1 Hz, 1H), 6.85–6.79 (m,

2H), 4.53 (d, J = 4.6 Hz, 1H), 4.49 (t, J = 5.4 Hz, 1H), 4.29 (s, 4H), 3.73 (s, 2H), 3.68

(dd, J = 10.9, 5.3 Hz, 1H), 3.38–3.34 (m, 1H), 2.39 (dd, J = 12.7, 7.2 Hz, 1H), 2.35 (s,

3H), 2.24 (s, 3H), 1.23 (s, 1H). ^{13}C NMR (151 MHz, DMSO-d_6) δ 160.12, 153.66,

147.79, 143.40, 142.99, 142.46, 137.11, 134.85, 134.72, 131.41, 126.98, 126.84,

126.68, 126.22, 122.54, 121.56, 120.22, 118.14, 117.18, 69.79, 64.92, 64.49 (2C),

60.63, 58.43, 42.91, 15.96. HRMS (ESI) for $C_{27}H_{29}N_5O_5$ [M + H]$^+$, calcd: 504.2241,

found: 504.2246. Purity, 98.7%.

6-(((2-Acetamidoethyl)amino)methyl)-*N*-(3-(2,3-dihydrobenzo[*b*][1,4]dioxin-6-yl)-2-methylphenyl)-[1,2,4]triazolo[4,3-*a*]pyridine-8-carboxamide (A25). White solid. Yield, 24%. Mp: 156.4–160.9 °C. ^{1}H NMR (600 MHz, DMSO-d_6) δ 11.38 (s, 1H), 9.16 (s, 1H), 8.75 (s, 1H), 8.53 (s, 1H), 8.15 (d, J = 8.0 Hz, 1H), 7.82 (s, 1H), 7.31 (t, J = 7.8 Hz, 1H), 7.06 (d, J = 7.5 Hz, 1H), 6.94 (d, J = 8.2 Hz, 1H), 6.85 (d, J = 1.8 Hz, 1H), 6.81 (dd, J = 8.2, 1.8 Hz, 1H), 4.30 (s, 4H), 3.91 (s, 2H), 3.16 (dd, J = 12.1, 6.1 Hz, 2H), 2.58 (t, J = 6.4 Hz, 2H), 2.36 (s, 3H), 1.80 (s, 3H). ^{13}C NMR (151 MHz, DMSO-d_6) δ 169.52, 160.14, 153.66, 147.65, 143.40, 142.99, 142.46, 137.11, 134.72, 134.52, 130.70, 129.73, 126.85, 126.68, 126.22, 122.54, 121.56, 120.23, 118.14, 117.18, 64.48 (2C), 49.22, 48.08, 39.05, 23.03, 15.96. HRMS (ESI) for $C_{27}H_{28}N_6O_4$ [M + H]$^+$, calcd: 501.2245, found: 501.2241. Purity, 99.0%.

N-(3-(2,3-Dihydrobenzo[*b*][1,4]dioxin-6-yl)-2-methylphenyl)-6-(((2-(methylsulfonamido)ethyl)amino)methyl)-[1,2,4]triazolo[4,3-*a*]pyridine-8-carboxamide (A26). White solid. Yield, 19%. Mp: 343.0–344.5 °C. ^{1}H NMR (600 MHz, DMSO-d_6) δ 11.38 (s, 1H), 9.18 (s, 1H), 8.76 (s, 1H), 8.53 (s, 1H), 8.15 (d, J = 8.0 Hz, 1H), 7.31 (t, J = 7.8 Hz, 1H), 7.06 (d, J = 7.5 Hz, 1H), 6.98 (s, 1H), 6.94 (d, J = 8.2 Hz, 1H), 6.85 (d, J = 1.8 Hz, 1H), 6.81 (dd, J = 8.2, 1.9 Hz, 1H), 4.30 (s, 4H), 3.92 (s, 2H), 3.08 (d, J = 5.3 Hz, 2H), 2.92 (s, 3H), 2.67 (t, J = 6.3 Hz, 2H), 2.36 (s, 3H). ^{13}C NMR (151 MHz, DMSO-d_6) δ 160.14, 153.66, 147.66, 143.40, 142.99, 142.46, 137.11, 134.72, 134.53, 130.72, 128.43, 126.85, 126.69, 126.23, 122.54, 121.56, 120.24, 118.14, 117.18, 64.49 (2C), 49.15, 48.33, 42.85, 40.43, 15.96. HRMS (ESI) for $C_{26}H_{28}N_6O_5S$ [M + H]$^+$, calcd: 537.1915, found: 537.1920. Purity, 98.6%.

N-(3-(2,3-Dihydrobenzo[*b*][1,4]dioxin-6-yl)-2-methylphenyl)-6-(((2-sulfamoy lethyl)amino)methyl)-[1,2,4]triazolo[4,3-*a*]pyridine-8-carboxamide (A27). White solid. Yield, 6%. Mp: 289.2–292.0 °C. ^{1}H NMR (600 MHz, DMSO-d_6) δ 11.45 (s, 1H), 9.47 (s, 1H), 8.76 (s, 1H), 8.29 (s, 1H), 8.14 (d, *J* = 7.9 Hz, 1H), 7.32 (t, *J* = 7.4 Hz, 1H), 7.07 (d, *J* = 7.7 Hz, 1H), 6.95 (d, *J* = 8.4 Hz, 1H), 6.86–6.73 (m, 4H), 4.30 (s, 4H), 3.86 (s, 2H), 3.19 (dd, *J* = 9.9, 5.6 Hz, 3H), 2.94 (t, *J* = 6.7 Hz, 2H), 2.36 (s, 3H). ^{13}C NMR (151 MHz, DMSO-d_6) δ 160.24, 147.07, 143.40, 142.99, 142.48, 137.78, 137.14, 134.73, 133.97, 129.74, 127.01, 126.77, 126.29, 126.21, 122.56, 121.75, 119.34, 118.14, 117.20, 64.48 (2C), 54.66, 49.03, 43.29, 15.95. HRMS (ESI) for $C_{25}H_{26}N_6O_5S$ [M + H]$^+$, calcd: 523.1758, found: 523.1766. Purity, 98.3%.

N-(2-Cyano-3-(2,3-dihydrobenzo[*b*][1,4]dioxin-6-yl)phenyl)-6-(((2-hydroxyet hyl)amino)methyl)-[1,2,4]triazolo[4,3-*a*]pyridine-8-carboxamide (A28). Off-white solid. Yield, 26%. Mp: 219.5–221.4 °C. ^{1}H NMR (600 MHz, DMSO-d_6) δ 11.99 (s, 1H), 9.21 (s, 1H), 8.74 (s, 1H), 8.55 (s, 1H), 8.31 (d, *J* = 8.2 Hz, 1H), 7.80 (t, *J* = 8.0 Hz, 1H), 7.39 (d, *J* = 7.6 Hz, 1H), 7.14 (s, 1H), 7.10 (d, *J* = 7.5 Hz, 1H), 7.03 (d, *J* = 8.3 Hz, 1H), 4.52 (s, 1H), 4.33 (s, 4H), 3.93 (s, 2H), 3.50 (d, J = 5.2 Hz, 2H), 2.62 (t, *J* = 5.5 Hz, 2H). ^{13}C NMR (151 MHz, DMSO-d_6) δ 160.94, 153.61, 147.48, 145.66, 144.54, 143.71, 141.71, 134.98, 134.15, 131.27, 130.03, 128.69, 126.47, 122.27, 121.94, 119.13, 117.87, 117.70, 116.41, 103.61, 64.60, 64.50, 60.81, 51.05, 49.41. HRMS (ESI) for $C_{25}H_{22}N_6O_4$ [M + H]$^+$, calcd: 471.1775, found: 471.1782. Purity, 99.2%.

N-(2-Cyano-3-(2,3-dihydrobenzo[*b*][1,4]dioxin-6-yl)phenyl)-6-(((2,3-dihydro

xypropyl)(methyl)amino)methyl)-[1,2,4]triazolo[4,3-*a*]pyridine-8-carboxamide

(A29). Pale-yellow solid. Yield, 10%. Mp: 269.5–273.4 °C. ^{1}H NMR (600 MHz, DMSO-d_6) δ 11.99 (s, 1H), 9.24 (s, 1H), 8.75 (s, 1H), 8.50 (s, 1H), 8.31 (d, J = 8.1 Hz, 1H), 7.79 (t, J = 7.6 Hz, 1H), 7.38 (d, J = 7.6 Hz, 1H), 7.15 (d, J = 11.4 Hz, 1H), 7.06 (dd, J = 44.5, 8.0 Hz, 2H), 6.76 (d, J = 7.1 Hz, 1H), 4.60 (d, J = 62.4 Hz, 2H), 4.33 (s, 4H), 3.74 (s, 2H), 3.69 (s, 1H), 2.55 (s, 1H), 2.40 (dd, J = 12.0, 6.9 Hz, 1H), 2.25 (s, 3H). ^{13}C NMR (151 MHz, DMSO-d_6) δ 160.89, 153.62, 147.62, 145.65, 144.53, 143.71, 141.71, 135.28, 134.13, 132.01, 131.26, 129.72, 126.99, 122.27, 119.14, 117.86, 117.69, 116.40, 115.60, 103.52, 69.79, 64.92, 64.60, 64.50, 60.61, 58.37, 42.90. HRMS (ESI) for $C_{27}H_{26}N_6O_5$ [M + H]$^+$, calcd: 515.2037, found: 515.2040. Purity, 99.1%.

6-(((2-Acetamidoethyl)amino)methyl)-*N*-(2-cyano-3-(2,3-dihydrobenzo[*b*][1, 4]dioxin-6-yl)phenyl)-[1,2,4]triazolo[4,3-*a*]pyridine-8-carboxamide **(A30).** Off-white solid. Yield, 20%. Mp: 182.5–187.4 °C. ^{1}H NMR (600 MHz, DMSO-d_6) δ 11.99 (s, 1H), 9.20 (s, 1H), 8.75 (s, 1H), 8.54 (s, 1H), 8.32 (s, 1H), 7.82 (s, 2H), 7.40 (s, 1H), 7.23–7.02 (m, 3H), 4.33 (s, 4H), 3.91 (s, 2H), 3.16 (s, 2H), 2.58 (s, 2H), 1.80 (s, 3H). ^{13}C NMR (151 MHz, DMSO-d_6) δ 169.54, 162.69, 160.92, 153.62, 147.48, 145.65, 144.53, 143.71, 141.71, 134.96, 134.15, 131.27, 128.54, 126.47, 122.27, 121.92, 119.15, 117.86, 117.70, 116.40, 103.60, 64.55, 49.18, 48.07, 36.16, 31.15, 23.02. HRMS (ESI) for $C_{27}H_{25}N_7O_4$ [M + H]$^+$, calcd: 512.2041, found: 512.2047. Purity, 98.5%.

_N_-(2-Cyano-3-(2,3-dihydrobenzo[*b*][1,4]dioxin-6-yl)phenyl)-6-(((2-(methylsu

lfonamido)ethyl)amino)methyl)-[1,2,4]triazolo[4,3-*a*]pyridine-8-carboxamide

(A31). White solid. Yield, 20%. Mp: 230.0–232.5 °C. ^{1}H NMR (600 MHz, DMSO-d_6) δ 12.00 (s, 1H), 9.23 (s, 1H), 8.75 (s, 1H), 8.55 (s, 1H), 8.32 (s, 1H), 7.80 (s, 1H), 7.40 (s, 1H), 7.06 (dd, *J* = 67.1, 30.1 Hz, 4H), 4.33 (s, 4H), 3.92 (s, 2H), 3.08 (s, 2H), 2.92 (s, 3H), 2.67 (s, 2H). ^{13}C NMR (151 MHz, DMSO-d_6) δ 162.69, 160.93, 153.63, 147.50, 145.66, 144.54, 143.72, 141.71, 134.99, 134.16, 131.26, 128.43, 126.48, 122.28, 121.95, 119.17, 117.87, 117.70, 116.41, 103.62, 64.50, 49.10, 48.30, 42.83, 36.16, 31.15. HRMS (ESI) for $C_{26}H_{25}N_7O_5S$ [M + H]$^+$, calcd: 548.1711, found: 548.1715. Purity, 98.7%.

In vitro PD-1/PD-L1 binding assay. The activities of compounds in inhibition of PD-1/PD-L1 interaction were evaluated by using the well-established HTRF assay. The PD-1/PD-L1 binding assay kit (64ICP01PEG) was purchased from Cisbio. The experiments were performed according to the instructions of the manufacturer, which could be obtained at https://www.cisbio.com/usa/drug-discovery/human-pd1pd-l1-biochemical-interaction-assay.

Determination of IFN-γ release. The T cell-tumor co-culture assay was conducted by ChemPartner. Briefly, Hep3B cells were engineered to stably express OS-8 (anti-CD3 single chain variable fragment) as well as human PD-L1 (hPD-L1). Fresh PBMCs were isolated from healthy donor. CD3 T cells were isolated from PBMCs by EasySep™ Human T Cell Isolation Kit (negative selection, STEMCELL Technologies). Hep3B/OS-8/hPDL1 cells were harvested and treated with 10 μg/mL

mitomycin C at 37 °C for 1.5h, and washed thoroughly with PBS. Hep3B/OS-8/hPDL1 and T cells ($2.5x10^4$ in 50 μL and $5x10^4$ in 100 μL complete media, respectively) were added to the 96-well plates, followed by the addition of 4x final concentration of test articles in 50 μL complete media according to the plate map, and co-culture at 37 °C, 5% CO_2 incubator for 3 days. The supernatants (150 μL) were harvested after 3 days of co-culture to determine IFN-γ levels.

Molecular docking. Molecular graphic manipulations and visualizations were performed using Discovery Studio Visualizer 4.0. AutoDock 4.2 was used as the docking program. The grid-enclosing box was placed on the centroid of the co-crystallized ligand. A 2.2-Å resolution structure of PD-L1 in a complex with compound **2** (PDB ID: 5J89) and a 1.7-Å resolution structure of PD-L1 in a complex with compound **6** (PDB ID: 5N2F) were taken from the protein data bank. The protein targets were prepared for the molecular docking simulation by removing the water molecules and bound ligands. Hydrogen atoms and Kollman charges were added to each protein atom. Each docking experiment was performed 200 times, thus yielding 200 docked conformations. All of the other parameters used in the docking process were set to default values. The model with the highest stabilization energy was used for further analysis.

ASSOCIATED CONTENT

Supporting Information

The Supporting Information is available free of charge on the ACS Publications website at DOI:

1
2
3
4
5
6
7
8
9
10
11
12
13
14
15
16
17
18
19
20
21
22
23
24
25
26
27
28
29
30
31
32
33
34
35
36
37
38
39
40
41
42
43
44
45
46
47
48
49
50
51
52
53
54
55
56
57
58
59
60

^{1}H NMR, ^{13}C NMR , and HPLC spectra of the target compounds

Molecular formula strings

AUTHOR INFORMATION

Corresponding Authors

*E-mail: qinmingze001@126.com (M.Q.)

*E-mail: yanfangzhao@126.com (Y.Z.)

*E-mail: gongpinggp@126.com (P.G.)

Notes

The authors declare no competing financial interest.

ABBREVIATIONS USED

PD-1, programmed cell death-1; PD-L1, programmed cell death-ligand 1; PD-L2, programmed death-ligand 2; IL-2, interleukin 2; IFN-γ, interferon-γ; NSCLC, non-small cell lung cancer; mAb, monoclonal antibody; VISTA, v-domain immunoglobulin-containing suppressor of T cell activation; BMS, Bristol-Myers Squibb; HTRF, homogenous time-resolved fluorescence; IC$_{50}$, half-maximal (50%) inhibitory concentration; SAR, structure-activity relationship; MeOH, methanol; EtOH, ethanol; DCM, dichloromethane; DMF, N,N-dimethylformamide; HATU,

2-(7-azabenzotriazol-1-yl)-*N,N,N′,N′*-tetramethyluronium hexafluorophosphate; DIPEA, *N,N*-diisopropylethylamine; PdCl$_2$(dppf), [1,1'-bis(diphenylphosphino)ferrocene]dichloropalladium(II); Pd(PPh$_3$)$_4$, tetrakis(triphenylphosphine)palladium(0); Pd(OAc)$_2$, palladium(II) acetate; PBMC, peripheral blood mononuclear cell.

REFERENCES

(1) Acurcio, R. C.; Scomparin, A.; Conniot, J.; Salvador, J. A. R.; Satchi-Fainaro, R.; Florindo, H. F.; Guedes, R. C. Structure-function analysis of immune checkpoint receptors to guide emerging anticancer immunotherapy. *J. Med. Chem.* **2018**, *61*, 10957−10975.

(2) Zou, W.; Chen, L. Inhibitory B7-family molecules in the tumour microenvironment. *Nat. Rev. Immunol.* **2008**, *8*, 467−477.

(3) Constantinidou, A.; Alifieris, C.; Trafalis, D. T.; Targeting programmed cell death-1 (PD-1) and ligand (PD-L1): A new era in cancer active immunotherapy. *Pharmacol. Therapeut.* **2019**, *194*, 84−106.

(4) Sun, C.; Mezzadra, R.; Schumacher, T. N.; Regulation and function of the PD-L1 checkpoint. *Immunity* **2018**, *48*, 434−452.

(5) Alsaab, H. O.; Sau, S.; Alzhrani, R.; Tatiparti, K.; Bhise, K.; Kashaw, S. K.; Iyer, A. K. PD-1 and PD-L1 checkpoint signaling inhibition for cancer immunotherapy: mechanism, combinations, and clinical outcome. *Front. Pharmacol.* **2017**, *8*, 1−15.

(6) Dermani, F. K.; Samadi, P.; Rahmani, G.; Kohlan, A. K.; PD-1/PD-L1 immune checkpoint: potential target for cancer therapy. *J. Cell Physiol.* **2018**, 1−13.

(7) Freeman, G. J.; Long, A. J.; Iwai, Y.; Bourque, K.; Chernova, T.; Nishimura, H.; Fitz, L. J.; Malenkovich, N.; Okazaki, T.; Byrne, M. C.; Horton, H. F.; Fouser, L.; Carter, L.; Ling, V.; Bowman, M. R.; Carreno, B. M.; Collins, M.; Wood, C. R.; Honjo, Tasuku. Engagement of the PD-1 immunoinhibitory receptor by a novel B7 family member leads to negative regulation of lymphocyte activation. *J. Exp. Med.* **2000**, *192*, 1027−1034.

(8) Barber, D. L.; Wherry, E. J.; Masopust, D.; Zhu, B.; Allison, J. P.; Sharpe, A. H.; Freeman, G. J.; Ahmed, R. Restoring function in exhausted CD8 T cells during chronic viral infection. *Nature* **2006**, *439*, 682−687.

(9) Teng, M. W. L.; Ngiow, S. F.; Ribas, A.; Smyth, M. J. Classifying cancers based on T-cell infiltration and PD-L1. *Cancer Res.* **2015**, *75*, 2139−2145.

(10) Kerr, K. M.; Tsao, M. S.; Nicholson, A. G.; Yatabe, Y.; Wistuba, I. I.; Hirsch, F. R. Programmed death-ligand 1 immunohistochemistry in lung cancer: in what state is this art? *J. Tohrac. Oncol.* **2015**, *10*, 985−989.

(11) Tan, T. H.; Pranavan, G.; Haxhimolla, H. Z.; Yip, D. New systemic treatment options for metastatic renal-cell carcinoma in the era of targeted therapies. *Asia-Pac. J. Clin. Onco.* **2010**, *6*, 5−18.

(12) Goodman, A.; Patel, S. P.; Kurzrock, R. PD-1-PD-L1 immune-checkpoint blockade in B-cell lymphomas. *Nat. Rev. Clin. Oncol.* **2017**, *14*, 203−220.

(13) Dosset, M.; Vargas, T. R.; Lagrange, A.; Boidot, R.; Vegran, F.; Roussey, A.; Chalmin, F.; Dondaine, L.; Paul, C.; Marie-Joseph, E. L.; Martin, F.; Ryffel, B.; Borg, C.; Adotevi, O.; Ghiringhelli, F.; Apetoh, L. PD-1/PD-L1 pathway: an adaptive

immune resistance mechanism to immunogenic chemotherapy in colorectal cancer. *Oncoimmunology* **2018**, *7*, e1433981.

(14) Guo, L.; Zhang, H.; Chen, B. Nivolumab as programmed death-1 (PD-1) inhibitor for targeted immunotherapy in tumor. *J. Cancer* **2017**, *8*, 410−416.

(15) Shaabani, S.; Huizinga, H. P. S.; Butera, R.; Kouchi, A.; Guzik, K.; Magiera-Mularz, K.; Holak, T. A.; Domling, A. A patent review on PD-1/PD-L1 antagonists: small molecules, peptides and macrocycles (2015-2018). *Expert Opin. Ther. Pat.* **2018**, *28*, 665−678.

(16) Wang, T.; Wu, X.; Guo, C.; Zhang, K.; Xu, J.; Li, Z.; Jiang, S. Development of inhibitors of the programmed cell death-1/programmed cell death-ligand 1 signaling pathway. *J. Med. Chem.* **2019**, *62*, 1715−1730.

(17) Chupak, L. S.; Zheng, X. Compounds Useful as Immunomodulators. WO2015034820, March 12, 2015.

(18) Chupak, L. S.; Ding, M.; Martin, S. W.; Zheng, X.; Hewawasam, P.; Connolly, T. P.; Xu, N.; Yeung, K.-S.; Zhu, J.; Langley, D. R.; Tenney, D. J.; Scola, P. M.; Mingo, P. A. Compounds Useful as Immunomodulators. WO2015160641, October 22, 2015.

(19) Yu, Z.; Wu, L.; Yao, W. Heterocyclic Compounds as Immunomodulators. US20180016260, January 18, 2018.

(20) Wu, L.; Yu, Z.; Zhang, F.; Yao, W. N-Phenyl-pyridine-2-carboxamide Derivatives and Their Use as PD-1/PD-L1 Protein/Protein Interaction Modulators. WO2017106634, June 22, 2017.

(21) Wu, L.; Zhang, F.; Mei, S.; Yao, W. Heterocyclic Compounds as

Immunomodulators. US2018057486, March 1, 2018.

(22) Lajkiewicz, N.; Wu, L.; Yao, W. Heterocyclic Compounds as Immunomodulators. US20170174679, June 22, 2017.

(23) Wu, L.; Shen, B.; Li, J.; Li, Z.; Liu, K.; Zhang, F.; Yao, W. Heterocyclic Compounds as Immunomodulators. US20170107216, April 20, 2017.

(24) Lange, C.; Malathong, V.; McMurtrie, D. J.; Punna, S.; Singh, R.; Yang, J.; Zhang, P. Immunomodulator Compounds. US2018008554, January 11, 2018.

(25) Zak, K. M.; Grudnik, P.; Guzik, K.; Zieba, B. J.; Musielak, B.; Dömling, A.; Dubin, G.; Holak, T. A. Structural basis for small molecule targeting of the programmed death ligand 1 (PD-L1). *Oncotarget* **2016**, *7*, 30323−30335.

(26) Guzik, K.; Zak, K. M.; Grudnik, P.; Magiera, K.; Musielak, B.; Torner, R.; Skalniak, L.; Domling, A.; Dubin, G.; Holak, T. A. Small-molecule inhibitors of the programmed cell death-1/programmed death-ligand 1 (PD-1/PD-L1) interaction via transiently induced protein states and dimerization of PD-L1. *J. Med. Chem.* **2017**, *60*, 5857−5867.

(27) Carter, L. L.; Fouser, L. A.; Jussif, J.; Fitz, L.; Deng, B.; Wood, C. R.; Collins, M.; Honjo, T.; Freeman, G. J.; Carreno, B. M. PD-1: PD-L inhibitory pathway affects both CD4^{+} and CD8^{+} T cells and is overcome by IL-2. *Eur. J. Immunol.* **2002**, *32*, 634−643.

(28) Seifert, A. M.; Zeng, S.; Zhang, J. Q.; Kim, T. S.; Cohen, N. A.; Beckman, M. J.; Medina, B. D.; Maltbaek, J. H.; Loo, J. K.; Crawley, M. H.; Rossi, F.; Besmer, P.; Antonescu, C. R.; DeMatteo, R. P. PD-1/PD-L1 blockade enhances T-cell activity and

antitumor efficacy of imatinib in gastrointestinal stromal tumors. *Clin. Cancer Res.* **2017**, *23*, 454−465.

(29) Chinai, J. M.; Janakiram, M.; Chen, F.; Chen, W.; Kaplan, M.; Zang, X. New immunotherapies targeting the PD-1 pathway. *Trends Pharmacol. Sci.* **2015**, *36*, 587−595.

(30) Konstantinidou, M.; Zarganes-Tzitzikas, T.; Magiera-Mularz, K.; Holak, T. A.; Dömling, A. Immune checkpoint PD-1/PD-L1: is there life beyond antibodies? *Angew. Chem. Int. Ed.* **2018**, *57*, 4840−4848.

(31) Zak, K. M.; Grudnik, P.; Magiera, K.; Dömling, A.; Dubin, G.; Holak, T. A. Structural biology of the immune checkpoint receptor PD-1 and its ligands PD-L1/PD-L2. *Structure* **2017**, *25*, 1163−1174.

1
2
3
4
5
6
7
8
9
10
11
12
13
14
15
16
17
18
19
20
21
22
23
24
25
26
27
28
29
30
31
32
33
34
35
36
37
38
39
40
41
42
43
44
45
46
47
48
49
50
51
52
53
54
55
56
57
58
59
60

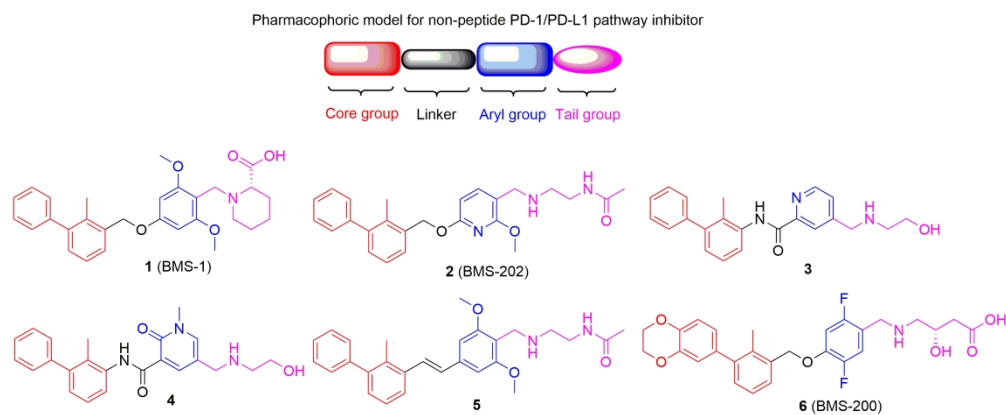**Table of Contents graphic**
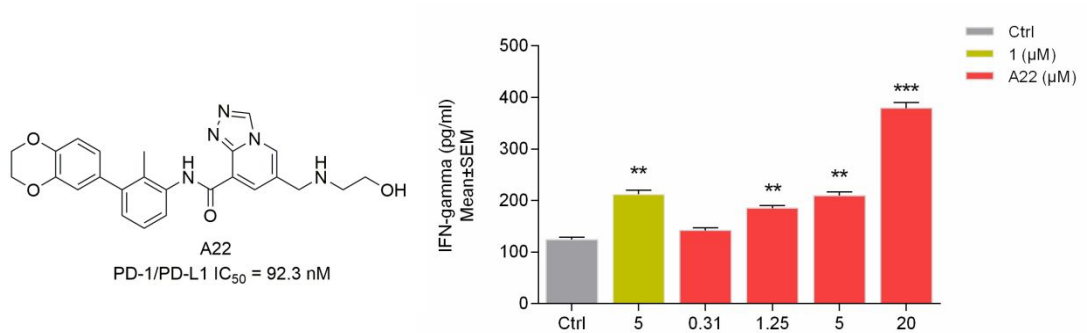
A22
PD-1/PD-L1 IC_{50} = 92.3 nM

Figure 1. Pharmacophoric model and chemical structures of non-peptide PD-1/PD-L1 pathway inhibitors.
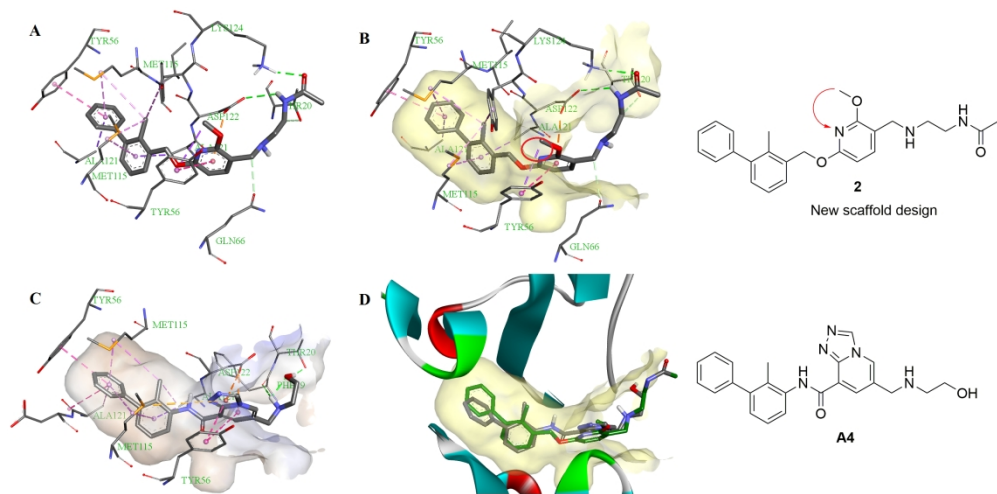
240x98mm (300 x 300 DPI)

Figure 2. (A) Detailed interactions of compound 2 with the dimeric PD-L1 protein. (B) Close-up view of compound 2 located in the hydrophobic cleft formed by the dimeric PD-L1 protein. (C) Docking analysis of A4 with the PD-L1 dimer. (D) Binding overlap of A4 and 2 in the binding site. The crystal structure of the dimeric PD-L1 protein was taken from the RCSB Protein Data Bank (PDB: 5J89).
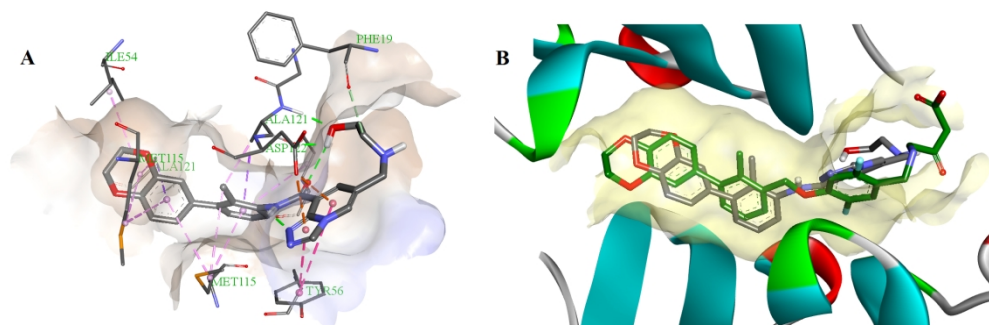
Figure 3. (A) Docking analysis of A22 with the PD-L1 dimer. (B) Binding overlap of A22 and 6 in the binding site. The crystal structure of the dimeric PD-L1 protein was taken from the RCSB Protein Data Bank (PDB: 5N2F).

1
2
3
4
5
6
7
8
9
10
11
12
13
14
15
16
17
18
19
20
21
22
23
24
25
26
27
28
29
30
31
32
33
34
35
36
37
38
39
40
41
42
43
44
45
46
47
48
49
50
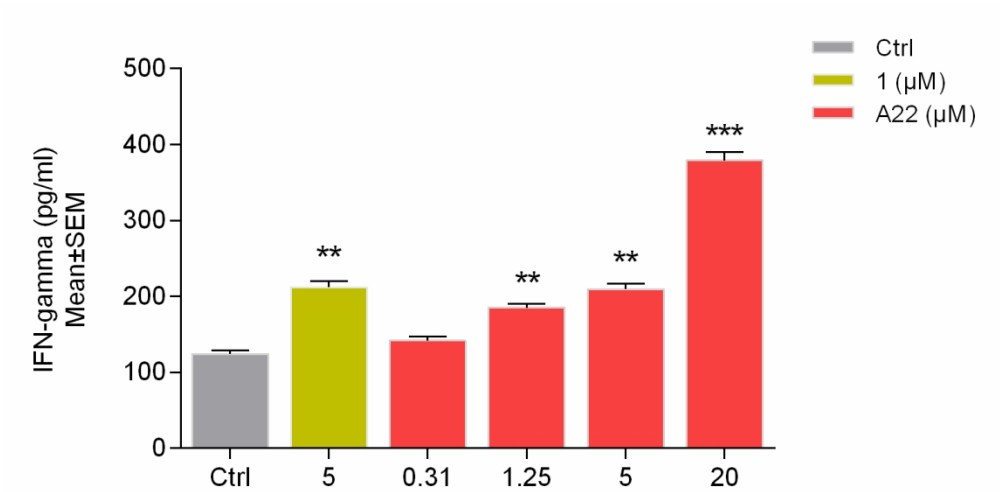51
52
53
54
55
56
57
58
59
60

Figure 4. Effects of compounds 1 and A22 on IFN-γ secretion from T cells co-cultured with tumor cells. Data are shown as mean ± SEM, *p<0.05, **p<0.01, *** p<0.001.

134x69mm (300 x 300 DPI)